

Distillation Decision Tree

Xuetao Lu ^a and J. Jack Lee ^{a*}

^a Department of Biostatistics, The University of Texas MD Anderson Cancer Center

* Author for correspondence: jjlee@mdanderson.org

Abstract

Machine learning models, particularly the black-box models, are widely favored for their outstanding predictive capabilities. However, they often face scrutiny and criticism due to the lack of interpretability. Paradoxically, their strong predictive capabilities suggest a deep understanding about the underlying data, implying significant potential for interpretation. Leveraging the emerging concept of knowledge distillation, we introduced the method of distillation decision tree (DDT). This method enables the distillation of knowledge about the data from a black-box model into a decision tree, thereby facilitating the interpretation of the black-box model. Constructed through the knowledge distillation process, the interpretability of DDT relies significantly on the stability of its structure. We establish the theoretical foundations for the structural stability of DDT, demonstrating that its structure can achieve stability under mild assumptions. Furthermore, we develop algorithms for efficient construction of (hybrid) DDTs. A comprehensive simulation study validates DDT's ability to provide accurate and reliable interpretations. Additionally, we explore potential application scenarios and provide corresponding case studies to illustrate how DDT can be applied to real-world problems.

Keywords: Knowledge distillation, Decision tree, Machine learning, Model interpretability, Prediction accuracy.

1 Introduction

In recent decades, machine learning (ML) has witnessed a remarkable surge in popularity and has found applications across a wide spectrum of domains. However, the widespread adoption of complex black-box ML models, such as neural networks and ensemble models, has led to growing concerns about their interpretability. This lack of interpretability has triggered skepticism and criticism, particularly in decision-based applications. For instance, in fields like medical diagnostics, the absence of interpretability could lead to erroneous diagnoses and potentially harmful treatment decisions. In these fields, linear models like linear regression or logistic regression are often preferred due to their interpretability. However,

their explanations tend to be relatively coarse and less precise when confronted with data exhibiting complex structures. This limitation arises from their simplistic structure, which is characterized by a fixed number of parameters. This simplicity can result in information loss, as reflected in their lower prediction accuracy. Higher prediction accuracy is indicative of a deeper understanding of the underlying structure of the data (Breiman, 2001). Black-box ML models typically outperform linear models in prediction accuracy, underscoring their potential to provide insightful interpretations of the data. Nonetheless, realizing this potential can be challenging because these black-box ML models are often too complex to be directly analyzed.

To address this challenge, we utilize the concept of knowledge distillation, which has gained widespread recognition in computer science community (Ba and Caruana, 2014; Hinton et al., 2015; Urban et al., 2017; Shi et al., 2019; Stanton et al., 2021; Allen-Zhu and Li, 2021). Originally introduced in the field of model compression, the primary purpose of knowledge distillation is to transfer knowledge from a complex model to a more lightweight one (Hinton et al., 2015). However, in our context, the objective is to interpret black-box ML models by distilling their knowledge about the data into a transparent model. Importantly, the knowledge distillation process can maintain the prediction accuracy of the transparent model at a level comparable to that of the black-box ML model. This guarantees that the transparent model possesses high-quality interpretability.

A decision tree emerges as an ideal choice for the transparent model (Johansson et al., 2011; Frosst and Hinton, 2017; Coppens et al., 2019; Li et al., 2020; Song et al., 2021; Ding et al., 2021) for two key reasons. Firstly, the decision tree model is inherently interpretable. Secondly, it possesses the capacity to capture complex data structures. Several studies have employed decision trees as transparent models alongside knowledge distillation. For instance, Frosst and Hinton (2017) explored the distillation of a neural network into a soft decision tree, while Coppens et al. (2019) discussed its application in interpreting deep reinforcement model, and Shen et al. (2020) used it for explaining data in the field of e-commerce. However, none of these studies considered the stability of decision trees constructed through knowledge distillation. The interpretability of decision trees relies heavily on the stability of their structure, which may be sensitive to the specific datasets used for training. Interpretations may become questionable if minor changes in the training data

significantly affect the tree’s structure. Given that the training data is generated randomly through the knowledge distillation process, ensuring the stability of the tree’s structure becomes a key challenge to address. While Zhou et al. (2018) explored tree structure stability in knowledge distillation, their study focused on a single splitting criterion and did not provide conclusive conditions under which the tree structure (or splits) converge. Therefore, a fundamental and comprehensive investigation of tree structure stability in the context of knowledge distillation is necessary.

In this paper, we introduce the term “distillation decision trees” (DDT) to refer to the decision trees generated through the knowledge distillation process. We offer both the theoretical foundations for ensuring the structural stability of DDT and practical algorithms for constructing it. We conduct a comprehensive theoretical examination of split stability, demonstrating that splits will converge in probability with a specific convergence rate, subject to mild assumptions. Our theoretical findings encompass the most commonly used splitting criteria and are applicable to both classification and regression problems. We propose and implement algorithms for (hybrid) DDT induction, along with parallelization strategies to mitigate computational demands. Through a simulation study, we validate DDT’s ability to provide precise interpretation while maintaining a stable structure, thus ensuring the credibility of its interpretations. Furthermore, we explore two application scenarios, each supported by corresponding case studies, to demonstrate the wide applicability of DDT.

The rest of the paper is organized as follows. In Section 2, we introduce the concepts and prerequisites of DDT. Section 3 then presents the theoretical foundations of split stability. Moving on to Section 4, we propose and implement algorithms for hybrid DDT induction, accompanied by discussions on sampling strategies. Section 5 presents the simulation study. Next, in Section 6, we delve into two application scenarios and corresponding case studies. Finally, we conclude and engage in a discussion in Section 7. Theoretical proofs and supplementary materials can be found in the Appendix. Additionally, an open-source R implementation of DDT is accessible on GitHub at <https://github.com/lxtpvt/ddt.git>.

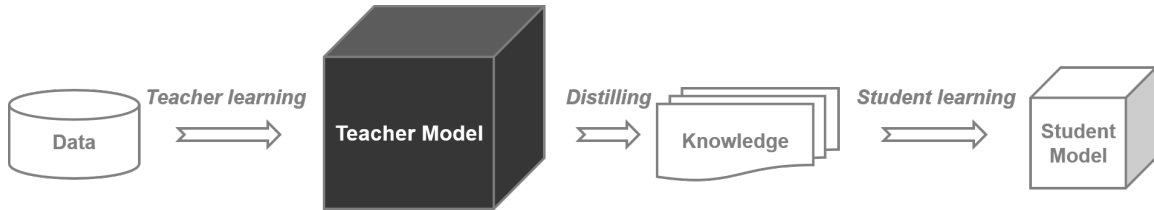


Figure 1: Knowledge distillation process.

2 Distillation Decision Tree

A distillation decision tree is essentially a decision tree. However, instead of being constructed directly from a dataset, it is generated from the knowledge distillation process, which could ensure the stability of the tree structure.

2.1 Knowledge Distillation Process

A typical knowledge distillation process is depicted in Figure 1. It begins with the training of the teacher model using the dataset, representing the teacher’s learning phase. Subsequently, the well-learned knowledge from the teacher model is distilled. Finally, the student model is trained using the distilled knowledge. This process can be adaptable to various scenarios. For instance, when distilling knowledge from deep neural networks, a lightweight neural network can serve as the student model (Gou et al., 2021). In this paper, we specify the components of this process as follows:

- **Data.** We denote the data as $D = \{Y, X\}$, where Y is the set of observations for the response variable y , X is the set of observations for the corresponding covariates $\mathbf{x} = (x_1, \dots, x_p)$. Both the response and covariates can be categorical or continuous variables.
- **Teacher model.** Although the teacher model can encompass various model types, we specifically define it as a black-box ML model for the purposes of this paper. We represent the teacher model as $y = f(\mathbf{x})$.
- **Knowledge.** The knowledge is generated through two steps: 1) random sampling of covariate values within their respective support, denoted as X' , and 2) generating the corresponding response values Y' using X' and the fitted teacher model, $f(X')$. This

phase is referred to as “distilling”, as illustrated in Figure 1. In this paper, we term the resulting random samples (knowledge) as pseudo data, denoted as $D' = \{Y', X'\}$.

- **Student model.** The student model is specifically defined as a decision tree and is referred to as a distillation decision tree (DDT). The process of constructing the DDT aligns with the “student learning” phase depicted in Figure 1.

2.2 Splitting Criteria

The selection of splitting criteria is crucial in constructing DDT. Typically, different criteria are used for regression and classification problems. In regression, the primary criterion often involves minimizing the sum of squared errors (SSE) or the mean squared error (MSE) after splitting, as defined below.

$$\min\left\{\sum_{i=1}^{n_l}(y_{li} - \bar{y}_l)^2 + \sum_{j=1}^{n_r}(y_{rj} - \bar{y}_r)^2\right\} \quad (1)$$

$$\min\left\{\frac{1}{n_l}\sum_{i=1}^{n_l}(y_{li} - \bar{y}_l)^2 + \frac{1}{n_r}\sum_{j=1}^{n_r}(y_{rj} - \bar{y}_r)^2\right\} \quad (2)$$

where the subscripts l, r represent the left and right node of a stump, $n_l + n_r = n$, $\bar{y}_l = \frac{1}{n_l}\sum_{i=1}^{n_l} y_{li}$ and $\bar{y}_r = \frac{1}{n_r}\sum_{j=1}^{n_r} y_{rj}$.

In classification, the common criterion for selecting the best split is to maximize the reduction in impurity after splitting, as defined below.

$$\max\{E - (E_l + E_r)\}, \quad (3)$$

where E is the total impurity before splitting, and E_l and E_r are the left and right sets of impurity after splitting.

However, widely used classification decision tree algorithms, such as ID3, C4.5 (Quinlan, 1993), and CART (Breiman et al., 1984), employ various impurity measures, including the Shannon entropy, gain ratio, and Gini index. The good news is that these measures can be unified within a framework using the Tsallis entropy (Wang and Xia, 2017), defined as follows.

$$E = S_q(Y) = \frac{1}{1-q}\left(\sum_{i=1}^C p(y_i)^q - 1\right), \quad q \in \mathbb{R}, \quad (4)$$

where Y is a random variable that takes value in $\{y_1, \dots, y_C\}$, $p(y_i)$ is the corresponding probabilities of y_i , $i = 1, \dots, C$, and q is an adjustable parameter. Let $q \rightarrow 1$, we can obtain the Shannon entropy (5).

$$ShEnt(Y) = \lim_{q \rightarrow 1} S_q(Y) = \lim_{q \rightarrow 1} \frac{1}{1-q} \left(\sum_{i=1}^C p(y_i)^q - 1 \right) = - \sum_{i=1}^C p(y_i) \ln(p(y_i)) \quad (5)$$

Let $q = 2$, we can get the Gini index (6).

$$GI(Y) = S_q(Y)_{q=2} = \frac{1}{1-2} \left(\sum_{i=1}^C p(y_i)^2 - 1 \right) = 1 - \sum_{i=1}^C p(y_i)^2 \quad (6)$$

As for the Gain ratio, it can be defined as (7).

$$GR(Y) = \frac{ShEnt(Y) - \frac{n_l}{n} ShEnt(Y_l) - \frac{n_r}{n} ShEnt(Y_r)}{ShEnt(\frac{n_l}{n}) + ShEnt(\frac{n_r}{n})}, \quad (7)$$

where Y_l and Y_r are the two data sets corresponding to the left and right child nodes. Therefore, the Gain ratio can also be expressed within the framework of Tsallis entropy by introducing a normalization factor with $q = 1$.

2.3 Split Search Algorithm

In addition to the splitting criteria, the split search algorithm also plays a crucial role in the construction of DDT. The most commonly used split search algorithm is the greedy search algorithm, which makes locally optimal choices at each stage in a heuristic manner, with the aim of finding a global optimum. The algorithm involves the following steps: (a) for each split, searching through all covariates; (b) for each covariate, searching through all values; (c) for each candidate pair (covariate, value), calculating the loss (or gain) defined by the splitting criteria; and (d) identifying the best split by minimizing the loss (or maximizing the gain). Although the greedy search algorithm may not always guarantee the global optimum, which is theoretically an NP problem (Hyafil and Rivest, 1976), we have chosen to use it in our study due to its widespread acceptance and practicality in the field.

3 Tree Structure Stability

In the knowledge distillation process, we can generate an arbitrarily large set of random pseudo data $D' = \{Y', X'\}$. Constructing a DDT with a stable structure based on D' is

feasible. However, directly studying the stability of an entire tree is challenging due to its complexity. A practical approach is to assess the stability of individual splits. This is because if all splits within a tree exhibit stability, it can be inferred that the entire tree is stable.

3.1 Split Convergence

We refer to a split as achieving stability when it converges. To conduct theoretical studies on split convergence, we introduce two assumptions as follows.

- (a) **Unary relationship.** Although the teacher model $f(\mathbf{x})$ has p -dimensional covariates $\mathbf{x} = (x_1, \dots, x_p)$, only one covariate is considered at each split. Therefore, a unary teacher model $f(x)$ that is used throughout Section 3.1 is defined as follows.

$$f(x) = f_k(x_k) = \int \dots \int f(\mathbf{x}) d\mathbf{x}_{\bar{k}}, \quad k = 1, \dots, p, \quad (8)$$

where $d\mathbf{x}_{\bar{k}} = \prod_{i \neq k} dx_i$. If x_j is categorical variables takes values in $\{1, \dots, C\}$, we set $\int f(\mathbf{x}_{\bar{j}}, x_j) dx_j = \sum_{l=1}^C f(\mathbf{x}_{\bar{j}}, x_j) I(x_j = l)$, where $\mathbf{x}_{\bar{j}}$ is the vector $\{x_i\}_{i \neq j}$, $I(\cdot)$ is an indicator function.

- (b) **Unique optimal split.** The split under consideration in Section 3.1 has a single optimal value associated with its corresponding covariate. Cases involving multiple optimal values will be discussed in Section 3.2. The definition of this optimal split can be found in Definition 3.1.

Definition 3.1 (Optimal split). Let Ω be the support of x , and $z_i^l(x)$ and $z_i^r(x)$ are functions $\Omega \rightarrow \mathbb{R}$, where $i = 1, \dots, C$ and C is a constant in \mathbb{N}^+ . Let $g(z_1^t(x), \dots, z_C^t(x))$ be a continuous function $\mathbb{R}^C \rightarrow \mathbb{R}$, where $t = l$ or r . Then, the optimal split $x_s \in \Omega$ is defined as follows.

$$x_s = \operatorname{argmin}_{x \in \Omega} [g(z_1^l(x), \dots, z_C^l(x)) + g(z_1^r(x), \dots, z_C^r(x))]. \quad (9)$$

There are four study scenarios, represented by combinations of variable types for x and y in Table 1. We will establish split convergence in all these scenarios. Before delving into that, we present Lemma 3.2 to simplify the proofs in scenarios 1 and 2.

Lemma 3.2. Assume $x \in [a, b]$, where $a, b \in \mathbb{R}$, be a continuous variable in the teacher model $y = f(x)$, and y can be a continuous or categorical variable. Let $z_c^l(x) = \int_a^x h_c^l(t) dt$,

Table 1: Study scenarios defined as combinations of variable types.

$x \backslash y$	Continuous	Categorical
Continuous	Scenario 1	Scenario 2
Categorical	Scenario 3	Scenario 4

$z_i^r(x) = \int_x^b h_c^r(t) dt$, where $h_c^l(\cdot)$ and $h_c^r(\cdot)$ are integrable functions in $[a, b]$, $c \in \{1, \dots, C\}$ and $C \in \mathbb{N}^+$. The function $g(\cdot) : \mathbb{R}^C \rightarrow \mathbb{R}$ is defined in Definition 3.1. Let x_s be the unique optimal split in (a, b) that is defined by (9).

Consider $\{x_1, \dots, x_{n-1}\}$ as $n - 1$ points drawn uniformly at random from the interval (a, b) , and arrange them in ascending order. Let $x_0 = a$ and $x_n = b$, and include them in $\{x_1, \dots, x_{n-1}\}$ to form the set $\{x_0, x_1, \dots, x_{n-1}, x_n\}$. Utilizing the teacher model, we can generate pseudo data as $\{(x_0, f(x_0)), (x_1, f(x_1)), \dots, (x_{n-1}, f(x_{n-1})), (x_n, f(x_n))\}$. Subsequently, we can fit a stump to the pseudo data by employing the greedy split search algorithm. The split criterion is defined as follows.

$$x_s^n = \underset{x_k, k \in \{1, \dots, n-1\}}{\operatorname{argmin}} [g(z_1^{l(n)}(x_k), \dots, z_C^{l(n)}(x_k)) + g(z_1^{r(n)}(x_{k+1}), \dots, z_C^{r(n)}(x_{k+1}))], \quad (10)$$

where, $z_c^{l(n)}(x_k) = \sum_{i=1}^k h_c^l(x_i) * \Delta_i$, $z_j^{r(n)}(x_{k+1}) = \sum_{j=k+1}^n h_c^r(x_j) * \Delta_j$ and $\Delta_i = x_i - x_{i-1}$, $i = 1, \dots, n$.

Let k_s^n denote the optimal integer k that minimized (10), in other world, $x_s^n = x_{k_s^n}$. Then, the following holds:

$$x_s^n \xrightarrow{P} x_s, \quad \text{as } n \rightarrow \infty.$$

The rate of convergence is $O(n^{-1})$.

See [proof](#) in Appendix A.

Scenario 1 : Both y and x are continuous variables.

Theorem 3.3 (Continuous split convergence under the criteria SSE). *Let X be a continuous random variable that takes values in $[a, b]$, where $a, b \in \mathbb{R}$. The teacher model $f(x)$ is integrable in $[a, b]$. We assume the existence of an unknown unique optimal split x_s in (a, b) , which is defined as follows:*

$$x_s = \underset{x \in (a, b)}{\operatorname{argmin}} \left[\int_a^x (f(t) - \mu_l(x))^2 dt + \int_x^b (f(t) - \mu_r(x))^2 dt \right], \quad (11)$$

where,

$$\mu_l(x) = \frac{1}{x-a} \int_a^x f(u) du \quad , \quad \mu_r(x) = \frac{1}{b-x} \int_x^b f(u) du.$$

Consider $\{x_1, \dots, x_{n-1}\}$ as $n-1$ points drawn uniformly at random from the interval (a, b) , and arrange them in ascending order. Let $x_0 = a$ and $x_n = b$, and include them in $\{x_1, \dots, x_{n-1}\}$ to form the set $\{x_0, x_1, \dots, x_{n-1}, x_n\}$. Utilizing the teacher model, we can generate pseudo data as $\{(x_0, f(x_0)), (x_1, f(x_1)), \dots, (x_{n-1}, f(x_{n-1})), (x_n, f(x_n))\}$. Subsequently, we can fit a stump to the pseudo data by employing the greedy split search algorithm and splitting criteria SSE in (1). Let x_s^n denote the split of the stump.

Then, 1) x_s^n converges to x_s in probability as $n \rightarrow \infty$. 2) The values of two fitted nodes converge to $\mu_l(x_s)$ and $\mu_r(x_s)$ in probability respectively as $n \rightarrow \infty$. 3) The rate of convergence is $O(n^{-1})$.

See [proof](#) in Appendix A.

Scenario 2 : y is a categorical variable and x is a continuous variable.

Theorem 3.4 (Continuous split convergence under the Tsallis entropy criteria). *Let X be a continuous random variable that takes values in $[a, b]$, where $a, b \in \mathbb{R}$. $y = f(x)$ is the teacher model. $Y = f(X)$ is a discrete random variable taking values $y \in \{y_1, \dots, y_C\}$, where $C \in \mathbb{N}^+$. Let $S_i = \{x | f(x) = y_i, x \in [a, b]\}$, $i = 1, \dots, C$. The probability mass function of Y in $[a, b]$ is that:*

$$p(y_i) = \int_{S_i} \frac{1}{b-a} dx, \quad i = 1, \dots, C.$$

And, the probability mass function of Y in $[a, x]$ is that:

$$p_{[a,x]}(y_i) = \int_{S_i \cap [a,x]} \frac{1}{x-a} dt.$$

Then, a Tsallis entropy can be calculated in $[a, x]$,

$$S_q([a, x]) = \frac{1}{1-q} \left(\sum_{i=1}^C p_{[a,x]}(y_i)^q - 1 \right), \quad q \in \mathbb{R}.$$

Assume the existence of an unknown unique optimal split x_s in (a, b) , which is defined as follows:

$$x_s = \underset{x \in (a,b)}{\operatorname{argmin}} [S_q([a, x]) + S_q([x, b])]. \quad (12)$$

Consider $\{x_1, \dots, x_{n-1}\}$ as $n - 1$ points drawn uniformly at random from the interval (a, b) , and arrange them in ascending order. Let $x_0 = a$ and $x_n = b$, and include them in $\{x_1, \dots, x_{n-1}\}$ to form the set $\{x_0, x_1, \dots, x_{n-1}, x_n\}$. Utilizing the teacher model, we can generate pseudo data as $\{(x_0, f(x_0)), (x_1, f(x_1)), \dots, (x_{n-1}, f(x_{n-1})), (x_n, f(x_n))\}$. Subsequently, we can fit a stump to the pseudo data by employing the greedy split search algorithm and splitting Tsallis entropy criteria in (3) and (4). x_s^n denotes the split of the stump.

Then, 1) x_s^n converges to x_s in probability as $n \rightarrow \infty$. 2) The rate of convergence is $O(n^{-1})$.

See [proof](#) in Appendix A.

Scenario 3 : y is a continuous variable and x is a categorical variable.

Theorem 3.5 (Categorical split convergence under MSE criteria). X is a discrete random variable taking values $x \in \{1, \dots, C_x\}$, where $C_x \in \mathbb{N}^+$. Y is a continuous random variable taking values $y \in [c, d]$, where $c, d \in \mathbb{R}$. Y has a finite mean μ . The conditional distribution of $Y|X$ is defined through the teacher model $y = f(x)$. The expectation of $Y|X$ is given by:

$$E(Y|X = k) = \mu_k, \quad k = 1, \dots, C_x \quad \text{and} \quad \mu = \frac{1}{C_x} \sum_{k=1}^{C_x} \mu_k. \quad (13)$$

Let us randomly sample n instances of X , denoted as $\{x_1, \dots, x_n\}$, from $\{1, \dots, C_x\}$. Corresponding samples of Y , denoted as $\{y_1, \dots, y_n\}$, are generated through the conditional distribution of $Y|X$. The uniform sampling assumption indicates $\lim_{n \rightarrow \infty} \frac{n_k}{n} = \frac{1}{C_x}$, where $n_k = \sum_{i=1}^n I(x_i = k)$, $k = 1, \dots, C_x$.

Assume the existence of an unknown unique optimal split x_s in $\{1, \dots, C_x\}$, which is defined as follows:

$$x_s = \operatorname{argmin}_{k \in \{1, \dots, C_x\}} \lim_{n \rightarrow \infty} \frac{1}{n} \left[\sum_{i=1}^{n_k} (y_{ki} - \mu_k)^2 + \sum_{l \neq k} \left(\sum_{j=1}^{n_l} (y_{lj} - \mu_{\bar{k}})^2 \right) \right], \quad (14)$$

where $\mu_{\bar{k}} = E(Y|X \neq k)$.

A stump can be fitted on the pseudo data $\{(x_1, y_1), \dots, (x_n, y_n)\}$ by using the greedy search algorithm and splitting MSE criteria in (2). Let x_s^n denote the split of the stump.

Then, 1) x_s^n converges to x_s in probability as $n \rightarrow \infty$. 2) The rate of convergence is $O(n^{-1})$.

See [proof](#) in Appendix A.

Scenario 4 : Both y and x are categorical variables.

Theorem 3.6 (Categorical split convergence under Tsallis entropy criteria). *X is a discrete random variable taking values $x \in \{1, \dots, C_x\}$, where $C_x \in \mathbb{N}^+$. Y is a discrete random variable taking values $y \in \{1, \dots, C_y\}$, where $C_y \in \mathbb{N}^+$. A joint distribution (X, Y) can be defined through the teacher model $y = f(x)$. Its probability mass function can be denoted as $p(x = i, y = j) = p_{ij}$, where $i = 1, \dots, C_x$, $j = 1, \dots, C_y$.*

Let us randomly sample n instances of X , denoted as $\{x_1, \dots, x_n\}$, from $\{1, \dots, C_x\}$. Corresponding samples of Y , denoted as $\{y_1, \dots, y_n\}$, are generated through the joint distribution (X, Y) . The uniform sampling assumption indicates $\lim_{n \rightarrow \infty} \frac{n_k}{n} = \frac{1}{C_x}$, where $n_k = \sum_{i=1}^n I(x_i = k)$, $k = 1, \dots, C_x$.

Assume the existence of an unknown unique optimal split x_s in $\{1, \dots, C_x\}$, which is defined as follows:

$$x_s = \underset{k \in \{1, \dots, C_x\}}{\operatorname{argmin}} [S_q(k) + S_q(\bar{k})], \quad (15)$$

where, $S_q(\cdot)$ is the Tsallis entropy,

$$S_q(k) = \frac{1}{1-q} \left(\sum_{j=1}^{C_y} (p_{kj})^q - 1 \right),$$

$$S_q(\bar{k}) = \frac{1}{1-q} \left(\sum_{j=1}^{C_y} \left(\sum_{i \neq k} p_{ij} \right)^q - 1 \right), \quad k, i \in \{1, \dots, C_x\}, \quad q \in \mathbb{R}.$$

A stump can be fitted with the pseudo data $\{(x_1, y_1), \dots, (x_n, y_n)\}$ by using the greedy search algorithm and the Tsallis entropy splitting criteria in (3) and (4). Let x_s^n denote the split of the stump.

Then, 1) x_s^n converges to x_s in probability as $n \rightarrow \infty$. 2) The rate of convergence is $O(n^{-1})$.

See [proof](#) in Appendix A.

Building upon the aforementioned theorems, we can now define the concepts of split convergence and tree convergence.

Definition 3.7 (Split convergence). Let x_s be a unique optimal split on Ω as defined in Definition 3.1. Suppose that $\{x_1, \dots, x_n\}$ are sampled uniformly at random from Ω . The

pseudo data $\{(x_1, y_1), \dots, (x_n, y_n)\}$ be generated using the teacher model $y = f(x)$. A stump is then fitted using this pseudo data. If the split of the stump converges to x_s in probability as the sample size $n \rightarrow \infty$, we refer to it as a convergent split.

Definition 3.8 (Tree convergence). In a fitted DDT, if all the splits converge in probability as the size of the pseudo data n approaches infinity, we can conclude that the DDT converges in probability as n goes to infinity.

3.2 Split Oscillation

In Section 3.1, we make the assumption that a stump has a unique optimal split value. However, it's important to note that this assumption doesn't always hold. In some cases, there may be a set of optimal split values, leading to what we refer to as split oscillation.

Definition 3.9 (Split oscillation). Suppose $\{x_1, \dots, x_n\}$ are sampled uniformly at random from $x \in \Omega$. The pseudo data $\{(x_1, y_1), \dots, (x_n, y_n)\}$ is generated using the teacher model $y = f(x)$. A stump is then fitted using this pseudo data. If, instead of converging to a unique optimal split, the split of the stump oscillates among a set of optimal splits as the pseudo data size $n \rightarrow \infty$, we refer to it as split oscillation.

Certain types of oscillation can be identified under the assumption that the greedy search algorithm can randomly select an optimal split from the set of all optimal splits. Figure 2 illustrates two typical identifiable oscillations that are relatively easy to detect. Their combinations can account for most practical cases of oscillation. However, we are not concerned with those that are rare or have little practical significance, such as situations where all points in Ω are optimal splits.

- (a) **Finite points.** There are m different optimal splits, x_{s1}, \dots, x_{sm} on Ω .
- (b) **An interval on a real line.** Let $x \in [a, b]$, $a, b \in \mathbb{R}$. Any split falling into an interval $[c, d] \in [a, b]$ is an optimal split.

Given our assumption that the greedy search algorithm randomly selects an optimal split, the final split follows a uniform distribution across the set of all optimal splits. In case (a), this distribution takes the form of a uniform discrete distribution with probability mass function $p(x_s) = p_i = 1/m$, where $i = 1, \dots, m$. In case (b), it corresponds to a continuous uniform distribution with probability density function $p(x_s) = 1/(x_{sr} - x_{sl})$, where

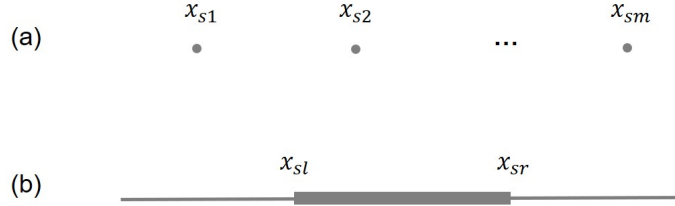


Figure 2: Two typical split oscillations. (a) Finite optimal splits. (b) Infinite optimal splits in an interval.

$x_s \in [x_{sl}, x_{sr}]$. Consequently, in practical applications, we can execute the greedy search algorithm a large number of times and analyze the empirical distribution to determine the type of oscillation.

3.3 Measure of Split Stability

We have established that the unique optimal split will converge as the pseudo sample size approaches infinity. However, in practice, only finite samples are available. Hence, we need a method to assess the stability of a split under a specific number of samples. Motivated by the greedy search algorithm, we propose two-level split stability (Figure 3) as follows.

- **First-level stability.** The first-level stability is defined as a discrete distribution with the probability mass function $p(x)$, which quantifies the stability of selecting covariate x_k ($k = 1, \dots, p$) as the splitting variable.
- **Second-level stability.** The second-level stability is defined as a conditional distribution, which is conditioned on the selected splitting covariate x_k . If x_k is a discrete variable, the second-level stability takes the form of a discrete distribution with the probability mass function $p(x_k)$. If x_k is a continuous variable, the second-level stability is expressed as a continuous distribution with the probability density function $f(x_k)$. (In Section 3.3, $f(\cdot)$ is used to represent a probability density function, not a teacher model.)

3.3.1 Measuring split stability in theory

In the case where x is continuous, we can derive certain theoretical results for the second-level stability by utilizing the proof presented in Lemma 3.2.

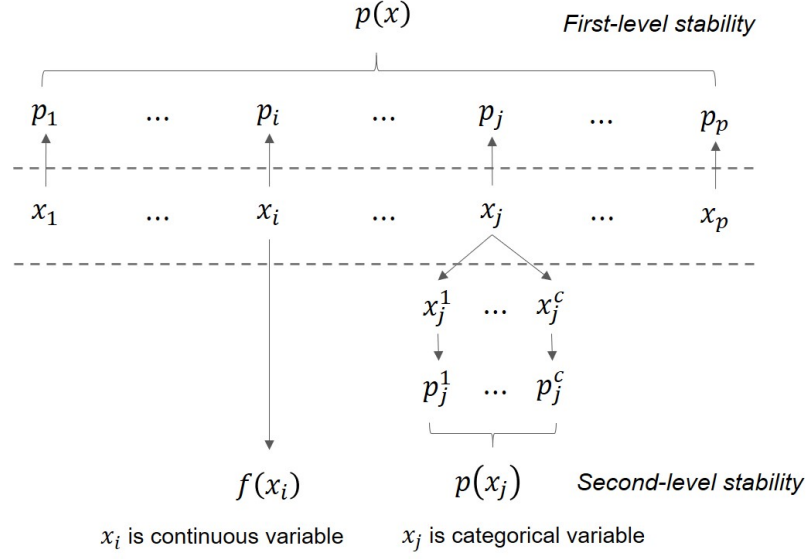


Figure 3: Two-level split stability. First-level stability is denoted as the discrete distribution of choosing a split variable. Second-level stability is denoted as the distribution of optimal split value, which can be a discrete or continuous distribution.

Proposition 3.10. Let x be a continuous variable taking values in $[a, b]$, $a, b \in \mathbb{R}$. Suppose x_s is the unique optimal split in (a, b) . Utilizing the set $\{x_0, x_1, \dots, x_{n-1}, x_n\}$, which is identical to the one in Lemma 3.2. let x_m represent the nearest point to x_s ,

$$|x_s - x_m| = \min\{|x_s - x_i|\}, \quad i = 1, \dots, n - 1.$$

Then, the probability of $|x_s - x_m| \leq d$ with $0 < d \leq \frac{b-a}{2}$ is as follows:

$$P(|x_s - x_m| \leq d) = 1 - \left(1 - \frac{2d}{b-a}\right)^n.$$

Proof. $P(|x_s - x_m| > d)$ indicates the probability of sample beyond the interval $[x_s - d, x_s + d]$. So,

$$P(|x_s - x_m| > d) = \left(1 - \frac{2d}{b-a}\right)^n.$$

Then, $P(|x_s - x_m| \leq d) = 1 - \left(1 - \frac{2d}{b-a}\right)^n$. □

A more practical interpretation of $P(|x_s - x_m| \leq d)$ is the probability that the true optimal split x_s lies within the interval $[x_m - d, x_m + d]$. In other words, the interval $[x_m - d, x_m + d]$ serves as the confidence interval for the true optimal split x_s at a significance

level of $\alpha = 1 - (1 - \frac{2d}{b-a})^n$. Unfortunately, neither x_s nor x_m are known. However, we do have knowledge about x_s^n . Referring to the proof of Lemma 3.2, we can deduce that:

$$x_s^n \xrightarrow{P} x_s, \quad x_m^n \xrightarrow{P} x_s \quad \text{as } n \rightarrow \infty,$$

such that

$$|x_s - x_m| \xrightarrow{P} |x_s - x_s^n| \quad \text{as } n \rightarrow \infty.$$

Moreover, Lemma 3.2 demonstrated that both x_m and x_s^n converge to x_s at the same rate. Therefore, it is reasonable to substitute x_m with x_s^n in the confidence interval $[x_m - d, x_m + d]$. Consequently, the interval $[x_s^n - d, x_s^n + d]$ can serve as an approximation for the $(1 - \alpha) * 100\% = (1 - \frac{2d}{b-a})^n$ confidence interval of the optimal split x_s .

Let $d = \frac{3(b-a)}{2n}$. We can obtain that,

$$\lim_{n \rightarrow \infty} [1 - (1 - \frac{2d}{b-a})^n] = \lim_{n \rightarrow \infty} [1 - (1 + \frac{-3}{n})^n] = 1 - e^{-3} \approx 0.950.$$

So, the interval

$$[x_s^n - \frac{3(b-a)}{2n}, x_s^n + \frac{3(b-a)}{2n}], \tag{16}$$

provides a good approximation of the 95% confidence interval for the true optimal split x_s when the sample size n is adequately large. This assertion is supported by the results of a simulation study presented in Appendix B. Furthermore, with a specified value for d , we can compute the necessary sample size to achieve a satisfactory approximation of the 95% confidence interval for the true optimal split x_s as follows,

$$n = \lceil \frac{3(b-a)}{2d} \rceil.$$

3.3.2 Measuring split stability via Monte Carlo simulation

Calculating the two levels of split stability analytically poses challenges, as their definitions are intricately connected to the greedy search algorithm, involving steps that resist translation into mathematical forms. Even the method outlined in Section 3.3.1, which theoretically calculates the second-level stability, can be challenging to implement in practice. For instance, obtaining the unary form $f(x)$ necessitates the computation of integrals as per Equation (8), when dealing with multiple covariates. Fortunately, Monte Carlo simulation offers a practical solution to perform these calculations.

Monte Carlo simulation allows us to estimate the first-level stability using the empirical probability mass function:

$$p(x_k) = p_k = \frac{n_k}{n}, \quad k = 1, \dots, p,$$

where n represents the number of simulations and n_k is the count of times that covariate x_k is selected as a split variable.

If x_k is a categorical variable with values x_k^1, \dots, x_k^C , the second-level stability can be estimated through the empirical probability mass function:

$$p(x_k^j) = p_k^j = \frac{n_k^j}{n_k}, \quad j = 1, \dots, C,$$

where n_k^j represents the number of times that value x_k^j is selected as a split value.

If x_k is a continuous variable, the second-level stability can be estimated through the empirical probability density function:

$$f(x_k) = \text{density}(X_k),$$

where X_k denotes the set of split values obtained from the Monte Carlo simulation, and $\text{density}(X_k)$ is a R function to estimate the empirical probability density function from the dataset X_k .

4 Algorithms for Constructing DDT

There are two fundamental distinctions in the construction of an ordinary decision tree (ODT) and a DDT. Firstly, ODT is built directly from a limited dataset, whereas DDT is constructed using an unlimited (in theory) sample of pseudo data. Secondly, ODT's primary aim is to best fit the dataset, whereas DDT's objective is to provide the best approximation of the teacher model. These distinctions result in the need for specific algorithms in constructing DDT compared to ODT.

4.1 Induction Algorithms

The most commonly used induction algorithm for constructing ODTs is a top-down recursive approach (Rokach and Maimon, 2014), referred to as the ODT induction algorithm in this paper. It starts with the entire input dataset in the root node, where a locally optimal

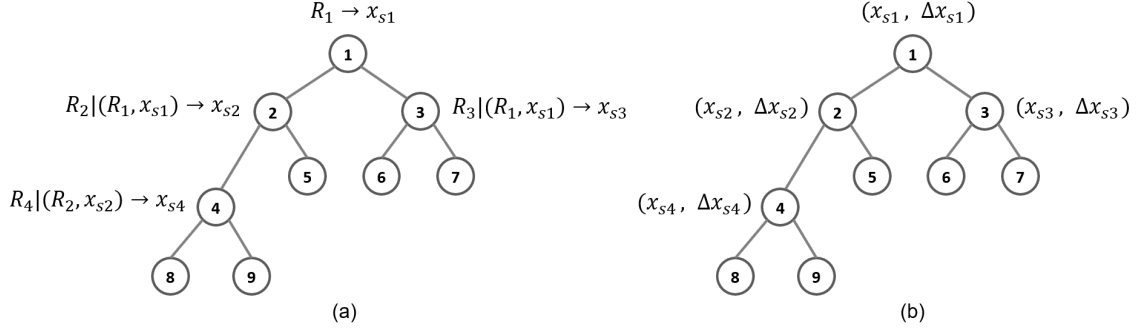


Figure 4: Examples of the dependency chain and variance propagation. (a) Two dependency chains in a tree. (b) The corresponding variance propagation.

split is identified using the greedy search algorithm, and conditional branches based on the split are created. This process is repeated in the generated nodes until the stopping criteria are met. A naive approach to construct a DDT is to directly apply the ODT induction algorithm on a large pseudo dataset. However, this method may not perform well in practice. Unlike the observed data used to fit ODTs, the pseudo data introduces variation (uncertainty) due to the random sampling process. This variation propagates in the constructed tree along dependency chains created by the top-down induction strategy. For instance, as illustrated in Figure 4 (a), the split x_{s4} depends on (R_2, x_{s2}) , which, in turn, depends on (R_1, x_{s1}) . The propagation of split variance follows the inverse direction of these dependencies. In Figure 4 (b), the variance Δx_{s1} will affect $(x_{s2}, \Delta x_{s2})$ and $(x_{s3}, \Delta x_{s3})$, and subsequently, Δx_{s2} will impact $(x_{s4}, \Delta x_{s4})$. This results in rapid inflation of variance as it propagates to deeper levels. For example, a small Δx_{s1} may lead to a substantial Δx_{s4} or even a change in the split variable.

To address the issue observed in the ODT induction algorithm, we have proposed Algorithm 1, which is referred to as the DDT induction algorithm in this paper. In the DDT induction algorithm, for a given node i , we measure its split N_i times. Utilizing these repeated measurements represented as X_s , we can calculate the two-level stability and choose a split value with the lowest variance. The first-level stability aids in reducing the variance when selecting the split variable, while the second-level stability assists in reducing the variance when identifying the split value. For example, if the split variable is continuous, and we opt for the mean of all fitted values, denoted as \bar{x}_s , the central limit theorem dic-

Algorithm 1: DDT induction algorithm

Data: Pseudo data

Result: A distillation decision tree

Starting from the root node, set $i = 1$, and create an empty set X_s to store splits.

while *stopping criteria are not met*, **do**

1. For node i , repeat the following processes N_i times.
 - (1) Generate pseudo data, which includes n_i samples from the sampling region R_i corresponding to node i .
 - (2) Fit a stump on the pseudo data and store the split of the stump into X_s .
2. Compute two-level stability with X_s to identify the best split x_s^* .
3. Apply x_s^* to create child nodes and set their id as $2i, 2i + 1$, respectively.
4. Move to the next node that needs to be split.

end

tates that the variance of \bar{x}_s will diminish at a rate of N_i^{-1} . By repeating this process at each split, we can construct a DDT with a stable structure. In practice, it is common to choose a reasonably large value for N_i (we typically set $N_i = 100$). The sample size n_i can be estimated in an ad-hoc manner based on the two-level stability through simulation. We determine the value of x_s^* by selecting the mode of the second-level stability (pmf/pdf). The stopping criteria can either be objective (e.g., a small distance, misclassification rate, or mean squared error in comparison to the teacher model) or subjective (e.g., a predefined number of nodes deemed sufficient for the intended application or explanation).

We assume that the teacher model is well-defined, meaning it fits the observed data well and does not suffer from overfitting issues. Given that one of DDT’s primary objectives is to provide the best approximation of the teacher model, methods used in ODTs to control model complexity, such as tree pruning, are unnecessary for DDT. Thus, in DDT construction, our main concern is striking the right balance between the degree of approximation and computational load. The DDT induction algorithm introduces the concept of

a sampling region, defined as follows.

Definition 4.1 (Sampling region). For node i in the DDT, its ancestor splits define a support of \mathbf{x} at this node. We denote it as R_i and refer to it as the sampling region of node i .

Sampling regions and the subsequent concept of sampling paths are crucial for the discussion in the following subsections.

Definition 4.2 (Sampling path). A sampling path is a series of nested sampling regions defined by the nodes in a DDT path. The sampling path $P_{i,j}$ starts from sampling region R_i and ends at sampling region R_j . In other words, $P_{i,j} = \{(R_i, \dots, R_j) | R_i \supset \dots \supset R_j\}$. Two sampling paths intersect if there exists a sampling region in one sampling path that includes any sampling region in the other sampling path.

4.2 Sampling Strategy

The DDT induction algorithm is conducted based on the pseudo data sampling. Various sampling strategies can be integrated with the DDT induction algorithm to achieve different goals.

(1) Breadth-first sampling strategy

Similar to the breadth-first search (BFS) algorithm (Cormen et al., 2009), the breadth-first sampling strategy begins at sampling region R_1 , corresponding to the root, and conducts sampling on all sampling regions at the current depth level before proceeding to regions at the next depth level. For instance, during the DDT induction illustrated in panel (a) of Figure 5, the breadth-first sampling strategy involves sampling the pseudo data in the following order: $\{R_1, R_2, R_3, R_4, R_6, R_8, R_{13}\}$.

(2) Path-based sampling strategy

Sampling can also be conducted along a specific sampling path, known as a path-based sampling strategy. This approach is employed when a particular sampling region is of interest, and it involves growing a branch rather than constructing an entire tree to conserve computational resources. For instance, in panel (a) of Figure 5, if our focus is on sampling within the region R_{13} , we don't need to build the entire tree; instead, we only need to expand a branch along the bold sampling path $P_{1,13} = \{R_1, R_3, R_6, R_{13}\}$.

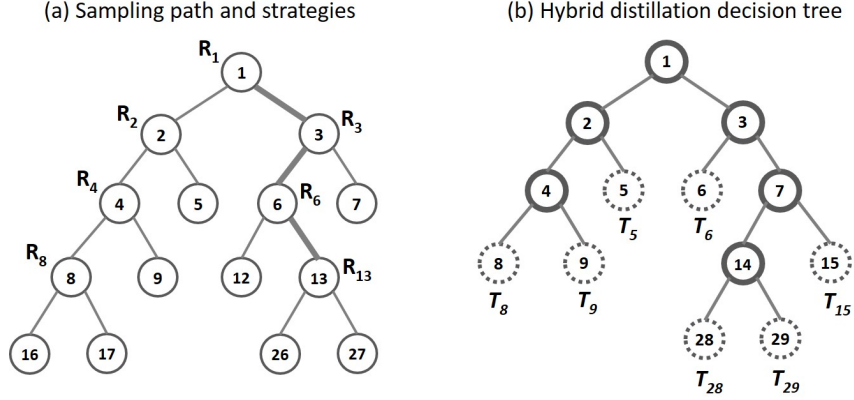


Figure 5: Sampling strategies and hybrid distillation decision tree. (a) An example for demonstrating the sampling path and discussing sampling strategies. (b) An example of the hybrid distillation decision tree.

(3) Parallel sampling strategy

The parallel sampling strategy involves simultaneously sampling several regions or paths to enhance the efficiency of the DDT induction algorithm. In general, when two sampling regions, denoted as R_i and R_j , cannot be connected through a sampling path $P_{i,j}$, parallel sampling in R_i and R_j becomes feasible. Tree structures are inherently conducive to parallel computing. For instance, parallel sampling can be applied at each level of the tree. In panel (a) of Figure 5, parallel sampling can occur in R_2 and R_3 at level one, R_4 and R_6 at level two, or R_8 and R_{13} at level three. This strategy can also be applied to sub-trees. Sub-trees rooted at nodes 2 and 3, for instance, can grow in parallel. Alternatively, parallel sampling can be implemented in sampling paths that do not intersect, such as the sampling paths $P_{2,8}$ and $P_{3,13}$.

4.3 Hybrid DDT

DDT induction Algorithm 1 requires repetitive sampling and fitting of data, performed N_i times to identify the best split. Each time, the pseudo data must have a sufficient size, leading to computationally intensive operations. Furthermore, to attain a high-quality approximation of the teacher model, the tree needs to grow to a considerable size. Consequently, growing a large DDT solely using the DDT induction Algorithm is often computationally infeasible.

Fortunately, in real-world applications, only a small subset of splits is typically needed for interpretation purposes. We refer to these splits as interpretable nodes (splits), while all other (leaf) nodes are considered predictive nodes. Consequently, it is reasonable to construct a hybrid DDT, which combines both DDT and ODT induction algorithms. Initially, we apply the DDT induction algorithm to the interpretable nodes, ensuring their two-level stability, which is crucial for interpretation. Subsequently, we employ the ODT induction algorithm to construct large sub-trees at the predictive nodes, maintaining a strong approximation of the teacher model. For instance, in panel (b) of Figure 5, the interpretable nodes are $\{1, 2, 3, 4, 7, 14\}$. We use the DDT induction algorithm to identify the stable splits for these nodes. Following this, we employ the ODT induction algorithm to grow the large sub-trees $\{T_5, T_6, T_8, T_9, T_{15}, T_{28}, T_{29}\}$ at the respective predictive nodes.

The importance of interpretation can vary among different interpretable nodes. Measuring and reporting these differences is crucial for explaining the teacher model and data based on these nodes (splits). To address this need, we introduce the concept of explanation index (XI). For predictive nodes, a similar index is calculated and referred to as the potential explanation index (PXI). The definitions of XI and PXI are provided below, and practical examples demonstrating their use can be found in Section 6.1.

Definition 4.3 (Explanation Index and Potential Explanation Index). The explanation index of interpretable node (split) i , denoted as XI_i , and the potential explanation index of predictive node j , denoted as PXI_j , are defined as follows:

$$\begin{aligned} XI_i &= \frac{\frac{n_i}{n} * \Delta_{S_i}}{\Delta_{DDT}} * 100\% \\ PXI_j &= \frac{\frac{n_j}{n} * \Delta_{T_j}}{\Delta_{DDT}} * 100\% \end{aligned} \tag{17}$$

where n_i , n_j , and n denote the number of observations in node i , subtree j , and the entire dataset. Δ_{T_j} and Δ_{S_i} represent the impurity reduction after fitting the split i or subtree j , respectively. $\Delta_{DDT} = \sum \frac{n_i}{n} * \Delta_{S_i} + \sum \frac{n_j}{n} * \Delta_{T_j}$.

Based on Definition 4.3, it is straightforward to verify that $\sum_i XI_i + \sum_j PXI_j = 1$. Furthermore, we can extend the concept of XI to apply to a path within DDT.

Definition 4.4 (Path Explanation Index).

$$XI_{ij} = \sum_{k \in S_{ij}} XI_k \tag{18}$$

where node i is an interpretable node, node j is a descendant of node i , and S_{ij} is a set of node IDs that encompasses the nodes in the path from node i to the parent of node j .

The small set of interpretable nodes enhances the simplicity of model interpretation. Meanwhile, the complexity necessary to ensure prediction accuracy comparable to that of the teacher model is achieved through the construction of large sub-trees at the predictive nodes. This decoupling between interpretability and complexity offers the potential for hybrid DDT to strike a balance between prediction accuracy and interpretability. For the sake of simplicity, the term “DDT” will refer to the hybrid DDT, and there will be no further distinction made in the remainder of this paper.

5 Simulation Study

The simulation study has three primary objectives: (1) to demonstrate the effectiveness of DDT in revealing intricate structures of the data, (2) to validate the interpretability of DDT, and (3) to illustrate the stability of interpretable splits (nodes).

To facilitate a clear and intuitive discussion, we introduce a two-dimensional function denoted as $y = f(x_1, x_2)$, consisting of 2601 data points, as illustrated in panel (a) of Figure 6. This function exhibits high non-linearity and intricate interactions, making it well-suited for our purposes. Let’s assume that $y = f(x_1, x_2)$ is unknown, as is often the case in practical situations. However, we can gain insights into its structure by analyzing the observations sampled from it. In panel (b), we have 50 observations randomly sampled from the true function. An ODT estimation fitted from these 50 observations is presented in panel (d). In comparison to the true function, the ODT estimation appears coarse and is unable to capture the intricate structure within the area marked by the green rectangle. In contrast, the random forest model provides a refined and precise estimation, as shown in panel (e). The DDT presented in panel (f), as a close approximation of its teacher, maintains a high-quality estimation comparable to the random forest model. This highlights the ability of the DDT to reveal intricate structures in the data.

For the function $y = f(x_1, x_2)$, effective interpretation is visually demonstrated through a suitable partition of the response values y based on the covariates x_1 and x_2 , as shown in panel (a) of Figure 6. This partition comprises nine splits generated by an ODT, the

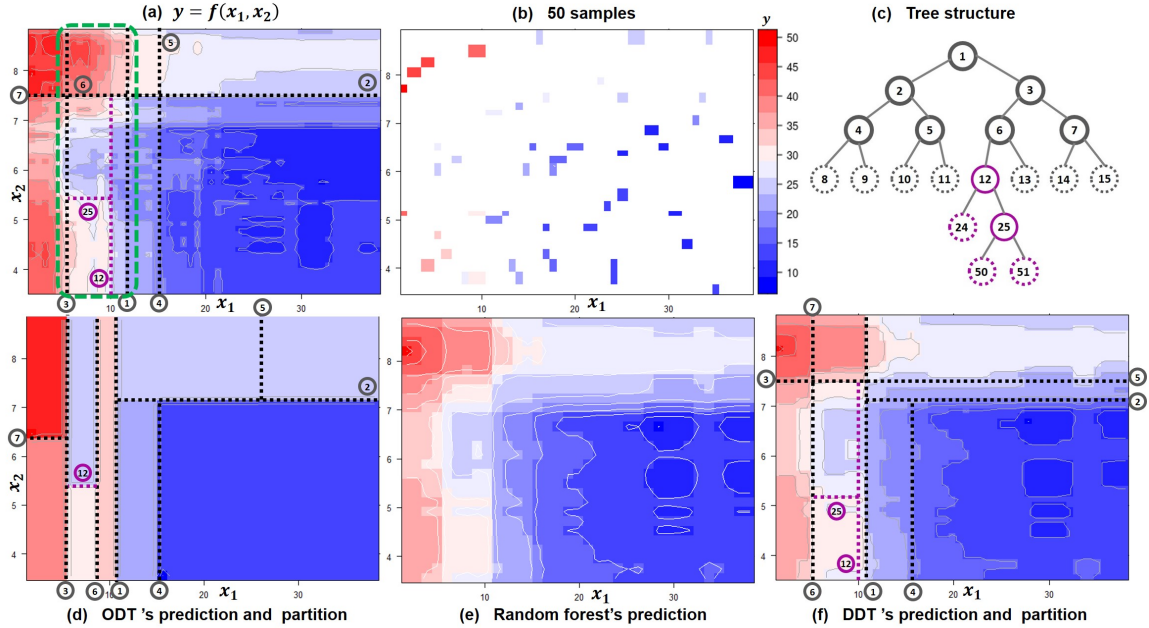


Figure 6: The effectiveness of DDT in revealing and explaining complex data structures. (a) The true function $y = f(x_1, x_2)$ and its partition with 9 splits. (b) 50 random samples from the true function. (c) The tree structure and splits for defining the partitions in (a), (d), and (f). (d) ODT is fitted based on the 50 samples. (e) RF is fitted based on the 50 samples. (f) DDT is built from the RF.

structure of which is depicted in panel (c). Since this ODT is fitted using the entire dataset of 2601 data points, we refer to this partition as the true partition, representing an optimal interpretation. Although the random forest model provides a highly accurate estimation of the true function, it cannot generate a partition for interpretation. The ODT is interpretable, but its interpretation (partition) is not accurate. In contrast, the DDT's interpretation (partition) closely approximates the optimal one (true partition), which is a good interpretation. However, this assessment relies on visual inspection, which can be challenging when verification is required numerous times. Figure 7 presents a quantitative method for comparing the quality of interpretation between ODT and DDT. Panel (a) displays the true partition (optimal interpretation). The partitions of ODT and DDT are depicted in panels (b-1) and (c-1), respectively. Panels (b-2) and (c-2) illustrate the absolute errors of ODT and DDT compared to the truth. Clearly, visual inspection still leads to the same conclusion that DDT's interpretation (partition) is superior to ODT's. More

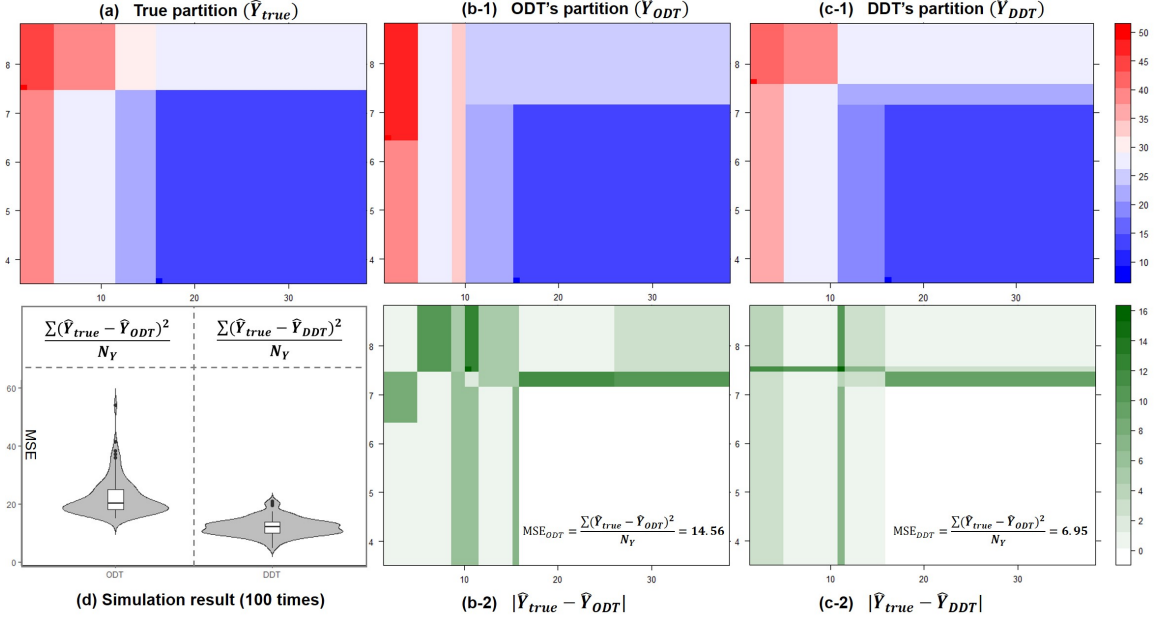


Figure 7: The comparison of interpretations and simulation result. (a) The true partition is obtained from the ODT that is fitted based on the entire data of the true function. (b-1) The ODT is fitted based on the 50 samples. (b-2) The result of $|\hat{Y}_{true} - \hat{Y}_{ODT}|$. (c-1) The DDT is built from RF. (c-2) The result of $|\hat{Y}_{true} - \hat{Y}_{DDT}|$. (d) MSE comparison of ODT and DDT with 100 times simulations.

importantly, we can quantify this difference using MSE. In this example, DDT's MSE is 6.95, significantly smaller than ODT's MSE of 14.56. Therefore, we can repeat this comparison 100 times. The result in panel (d) demonstrates that, in general, DDT outperforms ODT in terms of interpretation quality, thus validating the superior interpretability of DDT.

The DDT contains nine interpretable nodes (splits), as shown in panel (c) of Figure 6. Their first-level and second-level stability can be found in Figure 8. With the exception of split 12, which maintains a still impressive first-level stability of 97%, all other splits exhibit a first-level stability of 100%. Regarding second-level stability, each density function is tightly concentrated within a narrow interval and displays a sharp peak mode. Consequently, we can confidently assert that the interpretable splits within the DDT are highly stable.

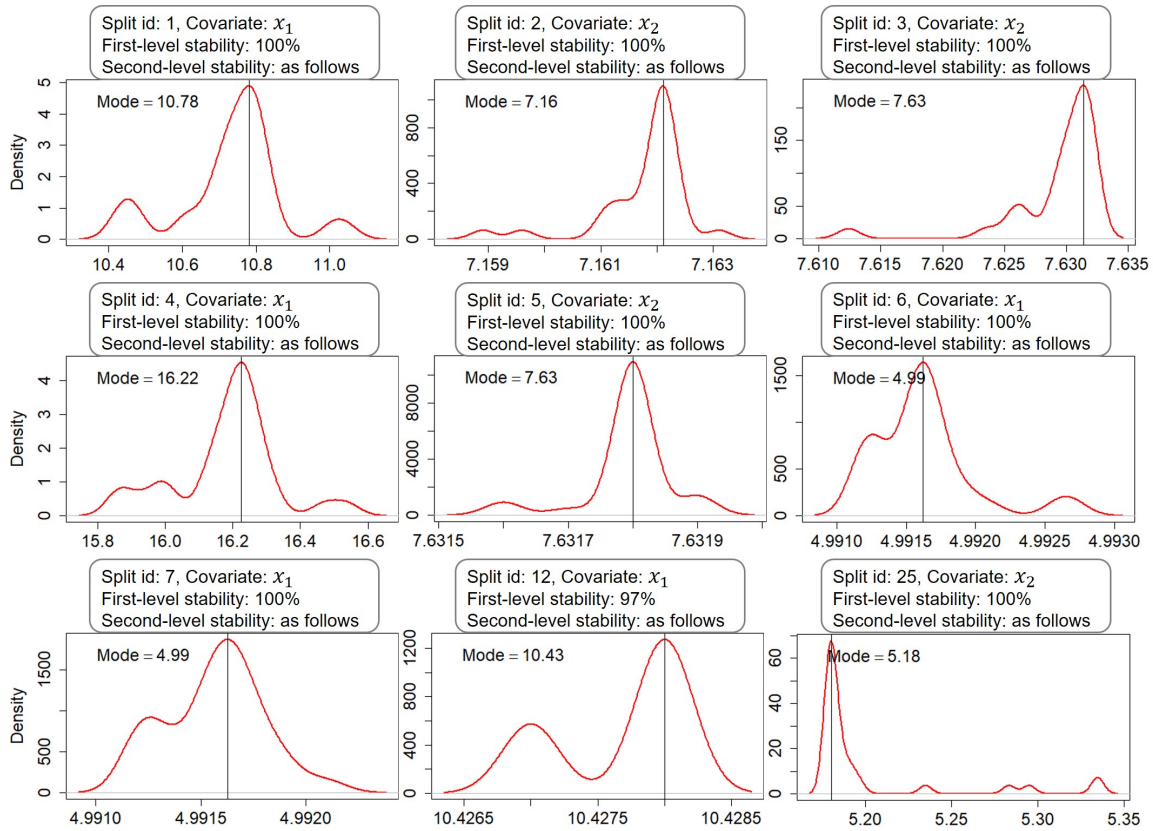


Figure 8: The two-level stability of interpretable splits in panel (f) of Figure 6.

6 Application Scenarios and Case Studies

When should we use DDT? There are two fundamental conditions that should be met.

- **Demands for understanding or explanation:** There is a need to understand or explain the data, either for personal insight or to communicate findings to others.
- **Possess good prediction accuracy:** The black-box ML model, which DDT aims to approximate, should outperform simple interpretable models, such as linear regression or ODT, in predicting the data. This suggests that the black-box model has a better understanding of the data's nature and has the potential to offer a more accurate interpretation than the simple models.

Considering these conditions, in this section, we discuss two application scenarios, each supported by corresponding case studies.

6.1 Model Interpretation

The dataset we used in the study cases of this application scenario is the Boston Housing dataset, which comprises a total of 506 observations. Each observation includes 14 variables, with the variable “medv” being the response variable of interest. The description of each variable is provided below:

medv: median value of owner-occupied homes in USD 1000’s.

crim: per capita crime rate by town.

zn: proportion of residential land zoned for lots over 25,000 sq.ft.

indus: proportion of non-retail business acres per town.

chas: Charles River dummy variable (= 1 if tract bounds river; 0 otherwise).

nox: nitric oxides concentration (parts per 10 million).

rm: average number of rooms per dwelling.

age: proportion of owner-occupied units built prior to 1940.

dis: weighted distances to five Boston employment centres.

rad: index of accessibility to radial highways.

tax: full-value property-tax rate per USD 10,000.

ptratio: pupil-teacher ratio by town.

b: $1000(B - 0.63)^2$ where B is the proportion of blacks by town.

lstat: percentage of lower status of the population.

As the second condition for using DDT, it is essential to confirm that the teacher model, which is the black-box ML model, can outperform simple interpretable models in terms of prediction accuracy. In this regard, we have selected the linear regression model (LM) and ODT as simple interpretable models, while considering the random forest (RF) and SVM as two candidates for the teacher model. Figure 9 displays the comparison of their prediction accuracy using a 5-fold cross-validation. It is evident that both RF and SVM outperform the simple interpretable models in both training and testing datasets. Furthermore, RF performs better than SVM. Hence, we opt for RF as the teacher model. We have also

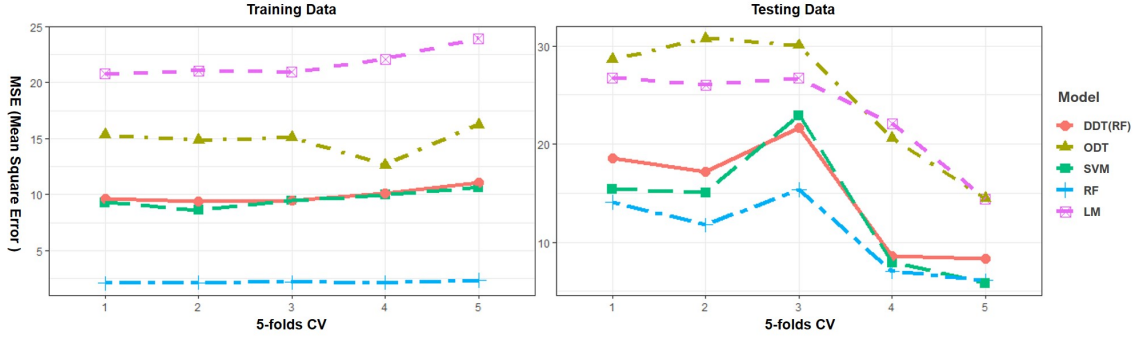


Figure 9: Comparison of prediction accuracy among ODT, LM, SVM, RF, and DDT (RF) on the training dataset (left) and testing dataset (right).

assessed the prediction accuracy of the fitted DDT(RF), and it closely approximates RF, exhibiting similar performance to SVM. As demonstrated in the simulation study, this strong prediction ability, which is comparable to its teacher model, enables DDT to offer a more accurate interpretation than the simple interpretable models.

The panel (a) of Figure 10 illustrates the interpretations provided by DDT(RF) for its teacher model RF. Since DDT(RF) is essentially a decision tree, calculating variable importance is straightforward. It reveals that the three most important variables are *lstat*, *rm*, and *nox*, representing social status, house size, and the natural environment, respectively. This is consistent with the variable importance results of the teacher model RF, as shown in Figure B.15 in Appendix B. The similarity between DDT(RF) and RF in terms of variable importance indicates that DDT can effectively provide an accurate interpretation for its teacher model. Variable importance is a valuable way of interpretation, although it tends to be somewhat generalized. More detailed and specific interpretations can be obtained by examining the interpretable splits (nodes) featured in panel (a). For example, if a house has seven or more rooms and is situated in an affluent community where the percentage of the population with lower social status (*lstat*) is less than 4.71%, it is likely to have a high value, averaging \$36,600 (in 1970). Additionally, for potential buyers, an intriguing insight emerges: they might acquire a larger house with seven or more rooms in a less affluent community with $lstat \geq 9.8\%$, priced around \$25,500, which is cheaper than a smaller house that could cost around \$26,300 in a community with $lstat \leq 9.7\%$. These specific insights are exemplified by nodes 5 and 6 in the tree.

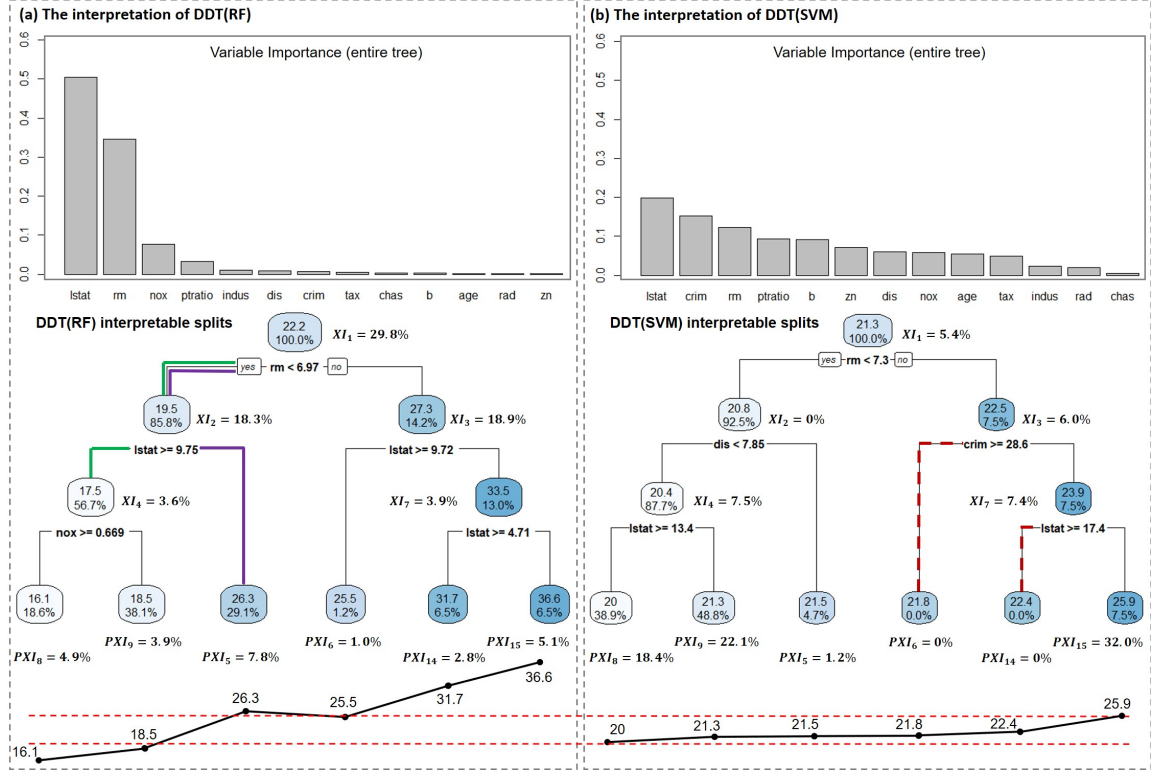


Figure 10: Model interpretation through DDT. (a) The interpretation of RF using DDT(RF). (b) The interpretation of SVM using DDT(SVM).

Within panel (a) of Figure 10, the XI and PXI values associated with the interpretable splits (nodes) and bottom predictive nodes provide relative importance information that enhances our understanding of the interpretation process. For instance, the high $XI_1 = 29.8\%$ for the split $rm < 6.97$ indicates the critical significance of whether a house has seven or more rooms in assessing its value. Moreover, these metrics can serve as criteria for identifying the set of interpretable nodes (splits). For example, we established the set of DDT(RF) interpretable splits by applying the criterion that all PXI must be less than 10%. This criterion ensures that predictive nodes do not contain substantial information requiring interpretation. The information referred to here represents the variation in impurity, which is denoted as MSE for regression and Tsallis entropy for classification. Furthermore, we can provide the XI to any prediction of DDT by using the concept of the path explanation index in Definition 4.4. For instance, if a prediction is made through the subtree (predictive node) 9 (see panel (a)), its XI can be calculated as $XI_{1,9} = XI_1 + XI_2 + XI_4 = 51.7\%$.

Then, with the $PXI_9 = 3.9\%$, we can offer a pair $(\frac{XI_{1,9}}{XI_{1,9}+PXI_9}, \frac{PXI_9}{XI_{1,9}+PXI_9}) = (93\%, 7\%)$. This pair indicates that this prediction can be interpreted with a degree of 93% using the rule chain $\{rm < 6.97 \rightarrow lstat \geq 9.75 \rightarrow nox \geq 0.669\}$.

Last but not least, the percentage of observed data displayed at each node also plays a pivotal role in comprehending the interpretation of DDT. This percentage serves as crucial evidence of how strongly the interpretation of a particular node is supported by the observed data. Given that DDT is not a direct interpretation of the observed data but rather of the teacher model, the support from the observed data is pivotal for the practical significance of the interpretation. Even a node (split) with a high XI may lack practical relevance if the percentage of observed data associated with it (or its children) is exceedingly low. For instance, consider node 6 (split 3), which boasts a high path XI of $XI_{1,6} = XI_1 + XI_3 = 48.7\%$ ($XI_3 = 18.9\%$). However, it (its left child) comprises a mere 1.2% of observed data. This suggests that the interpretation of this node (split) might not carry much practical importance. In other words, the real-world probability of purchasing a larger house at a lower price is not zero, but it is exceedingly low. Consequently, it is imperative to take into account both the XI and the percentage of observed data when interpreting DDT in practical applications. As an illustrative example, we can express confidence in the interpretation of predictions made through node (subtree) 9. Because this node not only has a high path XI of $XI_{1,9} = 51.7\%$ that can be interpreted with a degree of 93% but also enjoys strong practical support from a large number (38.1%) of observed data.

As demonstrated in panel (b) of Figure 10, DDT can also provide an interpretation for SVM, which differs from the one for RF. In DDT(SVM), the top three important variables are *lstat*, *crim*, and *rm*, representing social status, security, and house size, respectively. This indicates that, except for social status and house size, the SVM's explanation focuses on security, in contrast to the RF's emphasis on the natural environment. Regarding the interpretable splits, the sum of their XIs in DDT(SVM) is 26.3%, which is smaller than the 74.5% in DDT(RF). This suggests that the interpretable part of DDT(SVM) has a weaker interpretation compared to its counterpart in DDT(RF). The comparison of their predictions, as shown at the bottom of Figure 10, validates this assertion by indicating that DDT(RF) interprets more variations in the data than DDT(SVM). Another issue with DDT(SVM) is that splits 3 and 7 have child nodes 6 and 14, respectively, which do not

include any observed data. To address this, we can omit these two branches (colored with red dashed lines) and focus solely on node 15. The path explanation index from node 1 to 15 can then be calculated as $XI_{1,15} = XI_1 + XI_3 + XI_7 = 18.8\%$. In sum, through DDT, SVM can offer a different interpretation compared to RF. However, it's worth noting that the interpretable splits of DDT(SVM) do not perform as effectively as their counterparts in DDT(RF).

In the preceding case study, DDT was applied to interpret individual models like RF or SVM. However, DDT can also be valuable in interpreting models that are ensembled from multiple base models. One typical example is the Super Learner introduced by [Laan et al. \(2007\)](#). As depicted in panel (a) of Figure 11, the Super Learner employs cross-validation to estimate the performance of multiple (machine learning) base models. Subsequently, it constructs an optimal weighted average of these models based on their test data performance. This approach has been proven to yield predictions that are asymptotically as good as or even better than any single model within the ensemble. When applying this methodology to the BostonHousing dataset, we introduced eight base models and estimated their optimal weights for the Super Learner, as shown in panel (b) of Figure 11. Evaluated through a 10-fold cross-validation, the results presented in panel (c) of Figure 11 clearly demonstrate that the Super Learner outperforms all its base models in terms of prediction accuracy. This achievement satisfies the second condition necessary for the application of DDT.

Compared to the base models, the ensemble nature of the Super Learner introduces increased complexity, rendering it a somewhat more opaque black-box model, which can make its interpretation more challenging. However, DDT provides a viable solution to this challenge. Panel (d) of Figure 11 displays the variable importance results obtained from DDT(SL), which remarkably resemble those of the RF model shown in panel (a) of Figure 10. In panel (e) of Figure 11, interpretable splits (nodes) were selected based on the criterion that all PXIs should be less than 10%. The cumulative XIs for these splits amount to 75.2%, indicating that the interpretable part of DDT(SL) offers a substantial degree of interpretability. An interesting observation emerges when comparing DDT(RF) and DDT(SL): the predictions and interpretations of nodes 4 and 5 in DDT(RF) closely resemble those of nodes 4 and 6 in DDT(SL), respectively. In Figure 10 (a) and Figure 11

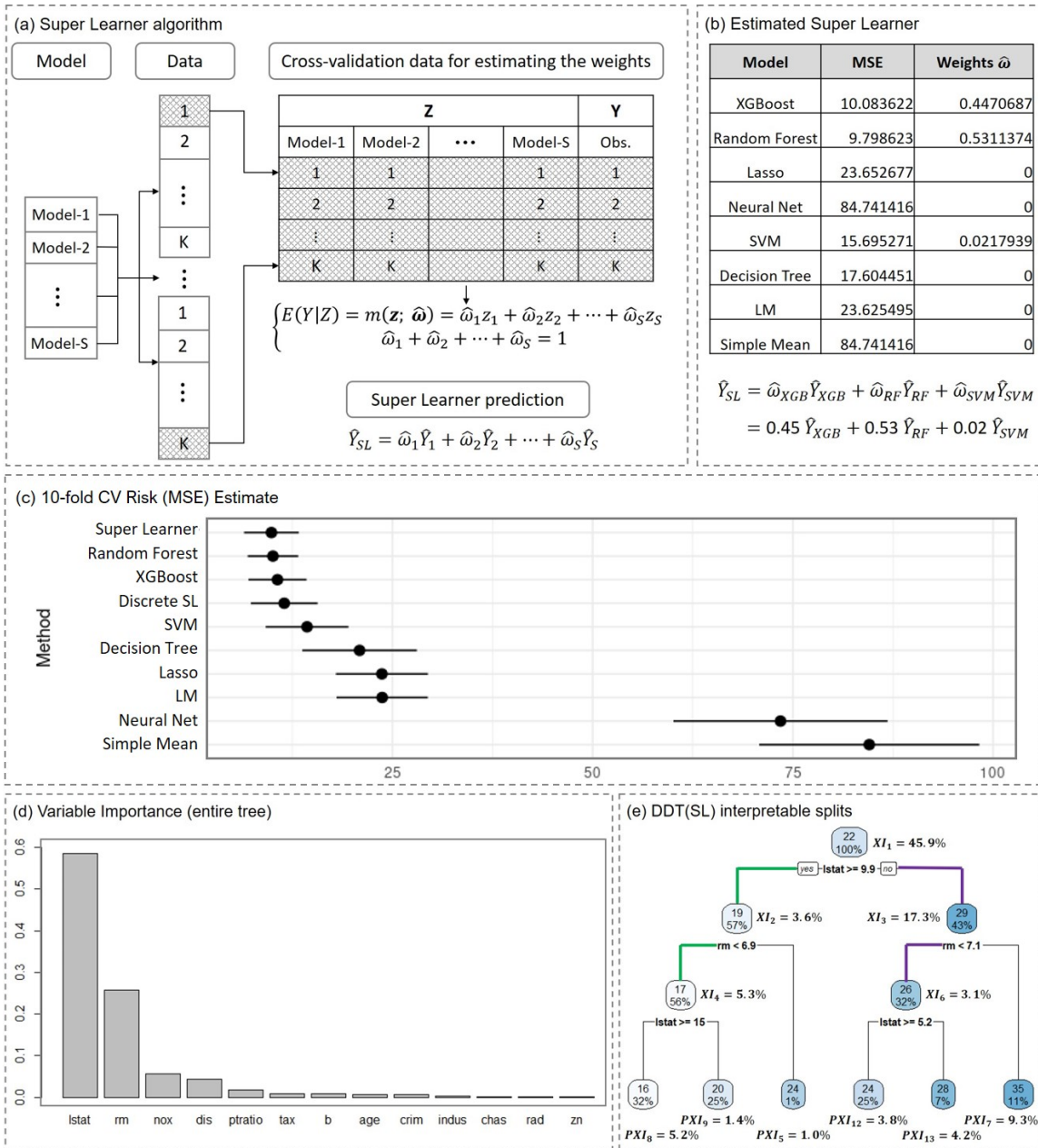


Figure 11: The interpretation of super learner through DDT. (a) The framework of super learner algorithm/model. (b) The estimated weights and super learner. (c) The comparison of prediction accuracy between super learner and base models. (d) and (e) The interpretations of super learner through DDT (SL).

(e), these corresponding paths are highlighted in green and purple, respectively. Notably, all of these compared paths exhibit both high explanation indices and substantial percentages of observed data. This suggests a strong similarity of interpretation between RF and the

Super Learner.

When you were a student, you might have encountered situations where your approach led to the correct answer but differed from the teacher’s. In such instances, teachers often reassure you by saying, ‘Don’t worry, all roads lead to Rome.’ Similarly, in the context of interpreting the BostonHousing dataset, we now have three DDT interpretations derived from corresponding black-box ML models. It’s important to emphasize that all of these interpretations are reasonable and valid. The choice among them depends on the specific application at hand. For example, consider a scenario where you are a real estate consultant serving different customers, each with their unique concerns. If one customer is primarily interested in the natural environment of the house, you might opt for the explanation provided by DDT(RF). On the other hand, if another customer’s main concern is the security of the neighborhood, you would choose the interpretation offered by DDT(SVM). In this way, you can tailor your interpretation to best suit the individual needs and priorities of your clients. Furthermore, if significant splits or rule chains consistently appear in different DDT interpretations, it serves as an indicator of their critical roles in understanding the data. These interpretations have the potential to provide valuable insights and knowledge about the data or application. For example, as discussed in the comparison of DDT(RF) and DDT(SL), we can derive the valuable insight that 10% lower status of the population and 7 rooms are two critical thresholds shaping people’s evaluations of house prices in Boston. (Note: The stability of splits for DDT(RF), DDT(SVM), and DDT(SL) can be found in Figure B.16 in Appendix B.)

6.2 Optimal Cutoff Identification and Subgroup Exploration

Traditional methods for subgroup identification typically rely on predefined variables and cutoffs. However, these methods come with challenges, (1) determining which variable should be chosen to define subgroups, (2) identifying the optimal cutoff value for the selected variable (3) multiplicity issues when testing multiple variables or cutoff values. To address these challenges, [Lipkovich et al. \(2017\)](#) introduced the concept of data-driven subgroup identification, which explores promising subgroups based on the inherent characteristics of the data, rather than relying on predefined variables and cutoffs. However, a drawback of existing data-driven methods is that subgroup identification is closely intertwined with

the data analysis method used. The quality of subgroup identification heavily depends on the quality of the chosen data analysis method. Since there is no single data analysis method that performs optimally on all datasets, this can be a limitation. DDT offers an innovative solution that decouples the processes of subgroup identification and data analysis. Researchers can initially select any model that best suits the dataset for data analysis and subsequently employ the corresponding DDT to explore and refine promising subgroups. This approach provides greater flexibility and adaptability compared to existing methods. Furthermore, the partitioning nature endows DDT with significant potential for identifying optimal cutoff values and uncovering meaningful subgroups.

For the case study in this application scenario, we utilized the WHAS (Worcester Heart Attack Study) dataset. The main goal of Worcester Heart Attack Study was to describe factors associated with trends over time in the incidence and survival rates following hospital admission for acute myocardial infarction. This dataset is available in the R package "mlr3proba" and comprises 481 observations. Each observation encompasses 14 variables. Four variables, namely id (Patient ID), year (Cohort year), yrgrp (Grouped cohort year), and dstat (Discharge status from the hospital: 1 = Dead, 0 = Alive), were excluded as they were not pertinent to the goal of study. The remaining variables are detailed below. lenfol and fstat correspond to the time and status variables used for survival analysis.

age: Age (per chart) (years).

sex: Sex. 0 = Male. 1 = Female.

cpk: Peak cardiac enzyme (iu).

sho: Cardiogenic shock complications. 1 = Yes. 0 = No.

chf: Left heart failure complications. 1 = Yes. 0 = No.

miord: MI Order. 1 = Recurrent. 0 = First.

mitype: MI Type. 1 = Q-wave. 2 = Not Q-wave. 3 = Indeterminate.

lenstay: Days in hospital.

lenfol: Total length of follow-up from hospital admission (days).

fstat: Status as of last follow-up. 1 = Dead. 0 = Alive.

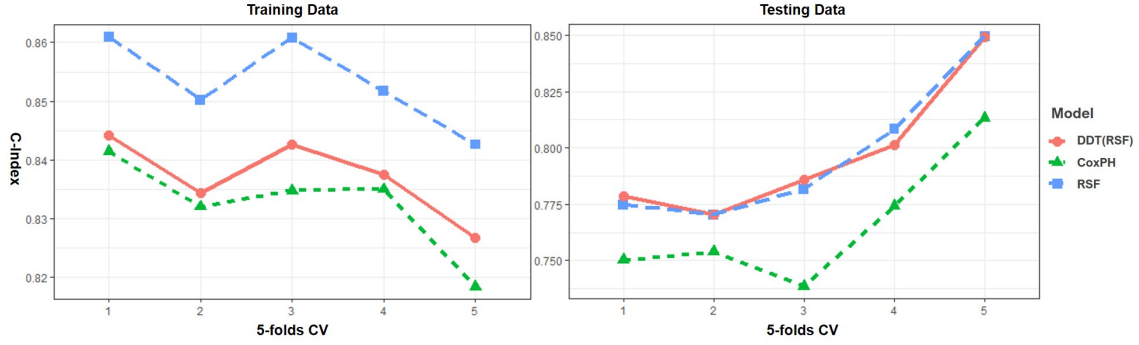


Figure 12: Comparison of prediction accuracy among CoxPH, RSF, and DDT (RSF) on the training dataset (left) and testing dataset (right).

To analyze this time-to-event dataset, we have two model options: a Random Survival Forest (RSF) model and a Cox Proportional Hazard (CoxPH) model. Figure 12 presents a comparison of their prediction accuracy using a 5-fold cross-validation. The C-index serves as the criterion, where a higher C-index signifies more accurate predictions. The results of the comparison clearly demonstrate that RSF outperforms CoxPH in prediction accuracy. This suggests that RSF is a superior choice as the data analysis model for this dataset. Furthermore, we also evaluated the prediction accuracy of the fitted DDT(RSF), finding that it closely approximates RSF’s performance, particularly in the testing dataset. This highlights the capability of DDT(RSF) as an effective model for subgroup identification.

To address the first challenge of variable selection for defining subgroups, the variable importance can provide valuable information. As illustrated in panel (a) of Figure 13, variable selection can follow an ascending order based on variable importance, with ”sho” \hat{c} ”age” \hat{c} ”chf,” and so forth. However, variable importance alone cannot provide information about the cutoff values. This is where the tree structure of DDT shines. Before delving into the details of subgroup identification with DDT, there are some important guidelines to keep in mind:

- The greedy search algorithm guides the split toward a locally optimal value, which can be considered a candidate for the optimal cutoff.
- The value of XI indicates the likelihood of selecting and the practical significance of a particular split variable and cutoff values. The greater the XI, the higher the likelihood of selecting that split variable and cutoff value, and they hold more practical

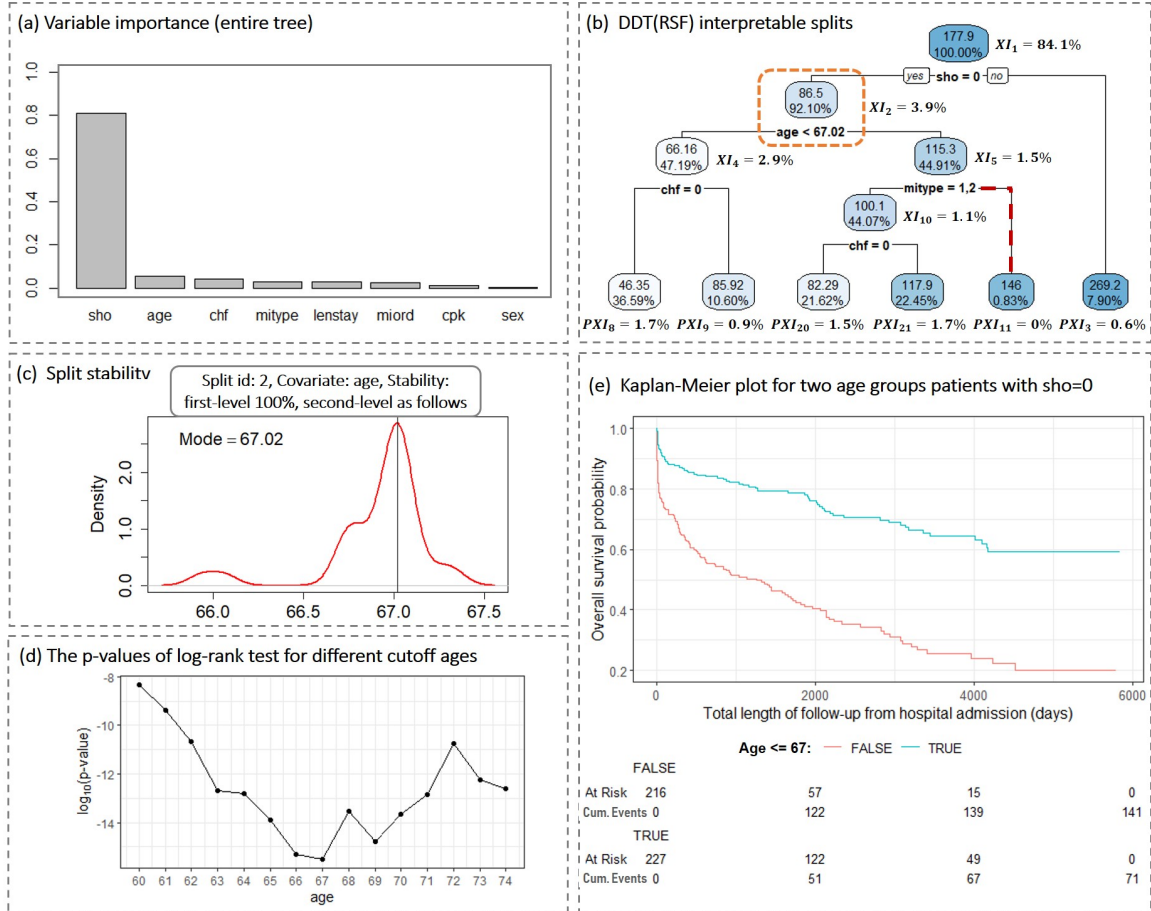


Figure 13: Optimal cutoff identification and subgroup exploration. (a) Variable importance provides information for selecting split variables. (b) Interpretable splits for identifying optimal cutoff and subgroups. (c) The two-level stability of split 2. (d) Log-rank tests for validating the optimality of cutoff value. (e) The Kaplan-Meier plot for the identified subgroups.

meaning.

- The observed data associated with the children nodes provides evidence for the practical significance of the parent split variable and its cutoff value. The more observed data and the more balanced allocation to left and right children, the stronger the evidence and support from observed data.

The structure of DDT(RSF) is depicted in panel (b) of Figure 13. The first split, sho=0, displays an exceptionally high $XI_1 = 84.2\%$, suggesting the great practical significance of the identified subgroups. However, due to the imbalance in the number of observed data between the left and right child, this practical significance is not strongly supported by the

Table 2: Subgroups identified by the splits of DDT(RSF) with the combinations of covariates, age and chf.

		age	
		≤ 67	> 67
chf	0	176	105
	1	51	111

observed data. Further investigation is needed, which might include hypothesis testing for statistical significance or expert knowledge for clinical significance. In practice, it is widely recognized that cardiogenic shock is positively associated with an increased risk of death. Consequently, while these two subgroups are practically meaningful, they might not be particularly interesting. The researcher’s interest may lie more in the subgroups identified from the patients who didn’t experience cardiogenic shock. In this case, the second split, $\text{age} < 67.02$, reveals two subgroups. The $XI_2 = 3.9\%$ suggests that these subgroups may not carry as much practical significance as those from the first split. Nevertheless, the observed data in child nodes are substantial and well-balanced, indicating strong support from the observed data and warranting further investigation. The stability of the optimal cutoff value is displayed in panel (c). The greedy search algorithm ensures the optimality of this cutoff value, which is substantiated by the p-values from log-rank tests across different cutoff values in panel (d). Consequently, there is no need to explore multiple cutoff values, thus alleviating the multiplicity issues. Panel (e) displays the Kaplan-Meier plot for the two subgroups, illustrating the varying risks associated with each subgroup.

Additional subgroups can be explored by conducting further splits. Since node 11 consists of only 4 observations, which represent 0.83% of the observed data, we can eliminate its parent node 5. This can be achieved by redistributing these 4 observations to nodes 20 and 21 based on their chf values. As a result, four distinct subgroups can be generated, with the number of patients in each subgroup outlined in Table 2. Analyzing this table reveals a clear trend: the risk of left heart failure ($\text{chf}=1$) tends to increase with age, indicating a dependency between chf and age. This relationship can be statistically confirmed through a χ^2 test, which yields a p-value of 2.655e-10.

7 Discussion

DDT offers a general method for interpreting black-box ML models. The primary challenge to the interpretation lies in constructing a stable DDT from the knowledge distillation process. We propose a comprehensive theory for split stability and develop efficient algorithms for constructing DDTs. In contrast to ODT, DDT exhibits a stable structure and can explore complex structures in the data, thereby delivering more detailed and precise interpretations.

DDT has significant potential in applications requiring interpretable models with strong predictive capabilities. We only discussed two application scenarios in this paper. Exploration of more real-world applications of DDT is a promising direction for future research. In our theory and algorithms, we employed the random sampling method to generate pseudo data for constructing DDT. This approach performed effectively in the simulation and application studies. Specifically, when dealing with sample sizes less than 60000, the time required to fit an interpretable node was under one minute. In general, for cases where the number of continuous covariates (n_{con}) remains relatively small, typically less than 10, the sample size of 60000 is sufficient. However, when dealing with larger n_{con} , a larger sample size is necessary. In such cases, random sampling can become inefficient. Therefore, another interesting direction for future research is the development of more efficient sampling strategies. Two promising strategies are MCMC sampling, which leverages information from the teacher model to enhance sampling efficiency, and PCA sampling, which employs dimension reduction to improve sampling efficiency.

[Bénard et al. \(2020\)](#) outlined simplicity, stability, and predictivity as essential requirements for interpretable models. For simplicity, DDT efficiently decouples the tasks of interpretation and prediction, maintaining a concise set of interpretable nodes for simplicity of use in interpretation. Stability, a central focus of this paper, is ensured through our theoretical results and construction algorithms, guaranteeing the stability of all interpretable splits (nodes). Regarding predictivity, DDT, as a closed approximation of black-box ML models, retains strong predictive performance comparable to the original black-box models. In conclusion, DDT is an excellent interpretable model with great potential for practical applications.

A Proofs

Proof of Lemma 3.2. There must exist a point x_m such that,

$$|x_s - x_m| = \min\{|x_s - x_i|\}, \quad i = 1, \dots, n-1.$$

Because x_i , $i = 1, \dots, n-1$ are uniformly distributed in (a, b) . For a constant ϵ , $0 < \epsilon < b - a$, by the theory of order statistics, it is easy to prove the following:

$$P(|x_s - x_m| > \frac{\epsilon}{2}) = (1 - \frac{\epsilon}{b-a})^n.$$

For any ϵ , $0 < \epsilon < b - a$,

$$\lim_{n \rightarrow \infty} P(|x_s - x_m| > \frac{\epsilon}{2}) = \lim_{n \rightarrow \infty} (1 - \frac{\epsilon}{b-a})^n = 0. \quad (19)$$

In other words, $x_m \xrightarrow{p} x_s$ as $n \rightarrow \infty$.

For any two consecutive points x_i and x_{i+1} , $i = 1, \dots, n$, and a constant ϵ , $0 < \epsilon < b - a$, we have that

$$P(|x_i - x_{i+1}| > \frac{\epsilon}{2}) = (1 - \frac{\epsilon}{b-a})^{n-1}.$$

Similar to (19), we can prove that $x_i \xrightarrow{p} x_{i+1}$ as $n \rightarrow \infty$. This also implies that $\Delta_i \xrightarrow{p} 0$ as $n \rightarrow \infty$ for $i = 1, \dots, n$.

Because $h(\cdot)$ is integrable in $[a, b]$ and $x_m \xrightarrow{p} x_s$, $\Delta_i \xrightarrow{p} 0$, as $n \rightarrow \infty$, we can get that

$$\lim_{n \rightarrow \infty} z_c^{l(n)}(x_m) = \lim_{n \rightarrow \infty} \sum_{i=1}^m h_c^l(x_i) * \Delta_i \xrightarrow{p} \int_a^{x_s} h_c^l(u) du = z_c^l(x_s). \quad (20)$$

Similarly, and by $x_{m+1} \xrightarrow{p} x_m \xrightarrow{p} x_s$, we can prove that,

$$\lim_{n \rightarrow \infty} z_c^{r(n)}(x_{m+1}) \xrightarrow{p} z_c^r(x_s).$$

Then, we can obtain that

$$\begin{aligned} & \lim_{n \rightarrow \infty} [g(z_1^{l(n)}(x_m), \dots, z_C^{l(n)}(x_m)) + g(z_1^{r(n)}(x_{m+1}), \dots, z_C^{r(n)}(x_{m+1}))] \\ & \xrightarrow{p} g(z_1^l(x_s), \dots, z_C^l(x_s)) + g(z_1^r(x_s), \dots, z_C^r(x_s)). \end{aligned} \quad (21)$$

Recall (10) and assume that

$$x_s^n \xrightarrow{p} x_s^*, \quad \text{as } n \rightarrow \infty.$$

Because $x_s^n = x_{k_s^n}$ and $x_{k_s^n+1} \xrightarrow{p} x_{k_s^n}$ as $n \rightarrow \infty$, we know that

$$x_{k_s^n} \xrightarrow{p} x_s^* \quad , \quad x_{k_s^n+1} \xrightarrow{p} x_s^*.$$

Using the integrability of $h(\cdot)$ and the same proof procedures of (20) and (21), we can obtain the following:

$$\begin{aligned} & \lim_{n \rightarrow \infty} [g(z_1^{l(n)}(x_{k_s^n}), \dots, z_C^{l(n)}(x_{k_s^n})) + g(z_1^{r(n)}(x_{k_s^n+1}), \dots, z_C^{r(n)}(x_{k_s^n+1}))] \\ & \xrightarrow{p} g(z_1^l(x_s^*), \dots, z_C^l(x_s^*)) + g(z_1^r(x_s^*), \dots, z_C^r(x_s^*)). \end{aligned} \quad (22)$$

According to the greedy search algorithm and split criterion in (10), for all $n \in \mathbb{N}$, we know that

$$\begin{aligned} & g(z_1^{l(n)}(x_m), \dots, z_C^{l(n)}(x_m)) + g(z_1^{r(n)}(x_{m+1}), \dots, z_C^{r(n)}(x_{m+1})) \\ & \geq g(z_1^{l(n)}(x_{k_s^n}), \dots, z_C^{l(n)}(x_{k_s^n})) + g(z_1^{r(n)}(x_{k_s^n+1}), \dots, z_C^{r(n)}(x_{k_s^n+1})). \end{aligned} \quad (23)$$

The equal sign holds if and only if $m = k_s^n$.

From (21), (22), and (23) we can get,

$$g(z_1^l(x_s), \dots, z_C^l(x_s)) + g(z_1^r(x_s), \dots, z_C^r(x_s)) \geq g(z_1^l(x_s^*), \dots, z_C^l(x_s^*)) + g(z_1^r(x_s^*), \dots, z_C^r(x_s^*)).$$

Since x_s is the unique and optimal split that satisfies the split criterion (9), the following must hold:

$$g(z_1^l(x_s), \dots, z_C^l(x_s)) + g(z_1^r(x_s), \dots, z_C^r(x_s)) \leq g(z_1^l(x_s^*), \dots, z_C^l(x_s^*)) + g(z_1^r(x_s^*), \dots, z_C^r(x_s^*)).$$

So,

$$g(z_1^l(x_s), \dots, z_C^l(x_s)) + g(z_1^r(x_s), \dots, z_C^r(x_s)) = g(z_1^l(x_s^*), \dots, z_C^l(x_s^*)) + g(z_1^r(x_s^*), \dots, z_C^r(x_s^*)),$$

and

$$x_s^n \xrightarrow{p} x_s^* = x_s, \quad \text{as } n \rightarrow \infty.$$

For the rate of convergence, let's recall (19) and change ϵ to $\frac{\epsilon'}{n}$, where ϵ' is a constant in $(0, b - a)$.

$$\lim_{n \rightarrow \infty} P(|x_s - x_m| > \frac{\epsilon'}{2n}) = \lim_{n \rightarrow \infty} (1 + \frac{-\epsilon'/(b-a)}{n})^n = e^{-\epsilon'/(b-a)}$$

Because $e^{-\epsilon'/(b-a)}$ is a constant, the convergence rate of x_m is $O(n^{-1})$.

Since $|x_s - x_s^n| \geq |x_s - x_m|$ always holds x_s^n converges to x_s slower or equal to x_m . However, by (23), we know that

$$g(z_1^{l(n)}(x_{k_s^n}), \dots, z_C^{l(n)}(x_{k_s^n})) + g(z_1^{r(n)}(x_{k_s^n+1}), \dots, z_C^{r(n)}(x_{k_s^n+1}))$$

converges to

$$g(z_1^l(x_s), \dots, z_C^l(x_s)) + g(z_1^r(x_s), \dots, z_C^r(x_s))$$

faster or equal than

$$g(z_1^{l(n)}(x_m), \dots, z_C^{l(n)}(x_m)) + g(z_1^{r(n)}(x_{m+1}), \dots, z_C^{r(n)}(x_{m+1}))$$

in all instances. This implies x_s^n converges to x_s faster or equal than x_m .

So, the convergence rate of x_s^n is exactly the same as x_m , and it is at the level $O(n^{-1})$ too. \square

Proof of Theorem 3.3. Construct that

$$\begin{aligned} g(z_c^l(x)) &= z_c^l(x), \quad g(z_c^r(x)) = z_c^r(x), \\ z_c^l(x) &= \int_a^x h_c^l(t) dt, \quad z_c^r(x) = \int_x^b h_c^r(t) dt, \\ h_c^l(t) &= (f(t) - \mu_l(x))^2, \quad h_c^r(t) = (f(t) - \mu_r(x))^2, \\ z_c^{l(n)}(x_k) &= \sum_{i=1}^k h_c^l(x_i) * \Delta_i, \quad z_c^{r(n)}(x_{k+1}) = \sum_{j=k+1}^n h_c^r(x_j) * \Delta_j, \end{aligned}$$

where $c = 1, \dots, C$ and $\Delta_i = x_i - x_{i-1}, i = 1, \dots, n$.

Under this construction, the optimal split x_s defined in (11) follows (9) in Definition 3.1. Obviously, $h_c^l(\cdot)$ and $h_c^r(\cdot)$ are integrable in $[a, b]$, because $f(\cdot)$ is integrable. So, by applying Lemma 3.2, x_s^n converges to x_s in probability and the rate of convergence is $O(n^{-1})$.

Since $f(\cdot)$ is integrable in $[a, b]$ and $x_{k_s^n+1} \xrightarrow{p} x_{k_s^n} = x_s^n \xrightarrow{p} x_s$, we can prove that

$$\begin{aligned} \lim_{n \rightarrow \infty} \frac{1}{x_{k_s^n} - a} \sum_{i=1}^{k_s^n} f(x_i) \Delta_i &\xrightarrow{p} \frac{1}{x_s - a} \int_a^{x_s} f(u) du = \mu_l(x_s), \\ \lim_{n \rightarrow \infty} \frac{1}{b - x_{k_s^n+1}} \sum_{j=k_s^n+1}^n f(x_j) \Delta_j &\xrightarrow{p} \frac{1}{b - x_s} \int_{x_s}^b f(u) du = \mu_r(x_s), \end{aligned}$$

and the rate of convergence is $O(n^{-1})$. \square

Proof of Theorem 3.4. Construct that

$$\begin{aligned}
g(z_1^l(x), \dots, z_C^l(x)) &= \frac{1}{1-q} \left(\sum_{c=1}^C z_c^l(x)^q - 1 \right), \\
g(z_1^r(x), \dots, z_C^r(x)) &= \frac{1}{1-q} \left(\sum_{c=1}^C z_c^r(x)^q - 1 \right), \\
h_c^l(t) &= \frac{1}{x-a} * I_{y_c}(f(t)), \quad h_c^r(t) = \frac{1}{b-x} * I_{y_c}(f(t)), \\
z_c^l(x) &= \int_a^x h_c^l(t) dt = \int_a^x \frac{1}{x-a} * I_{y_c}(f(t)) dt = \int_{S_i \cap [a,x]} \frac{1}{x-a} dt = p_{[a,x]}(y_c), \\
z_c^r(x) &= \int_x^b h_c^r(t) dt = \int_x^b \frac{1}{b-x} * I_{y_c}(f(t)) dt = \int_{S_i \cap [x,b]} \frac{1}{b-x} dt = p_{[x,b]}(y_c), \\
z_c^{l(n)}(x_k) &= \sum_{i=1}^k h_c^l(x_i) * \Delta_i = \frac{1}{x-a} \sum_{i=1}^k \Delta_i * I_{y_c}(f(x_i)), \\
z_c^{r(n)}(x_{k+1}) &= \sum_{j=k+1}^n h_c^r(x_j) * \Delta_j = \frac{1}{b-x} \sum_{j=k+1}^n \Delta_j * I_{y_c}(f(x_j)),
\end{aligned}$$

where $c = 1, \dots, C$, $\Delta_i = x_i - x_{i-1}$, $i = 1, \dots, n$ and $I_{y_c}(f(x))$ is an indicator function that is equal to 1 at $f(x) = y_c$ and 0 elsewhere.

Under this construction, the optimal split x_s defined in (12) follows (9) in Definition 3.1. Obviously, $h_c^l(\cdot)$ and $h_c^r(\cdot)$ are integrable in $[a, b]$. So, by applying Lemma 3.2, x_s^n converges to x_s in probability and the rate of convergence is $O(n^{-1})$. \square

Proof of Theorem 3.5. Let's construct that

$$\lim_{n \rightarrow \infty} \frac{1}{n} \sum_{i=1}^{n_k} (y_{ki} - \mu_k)^2 = z^l(k), \quad \lim_{n \rightarrow \infty} \sum_{l \neq k} \left(\sum_{j=1}^{n_l} (y_{lj} - \mu_{\bar{k}})^2 \right) = z^r(k) \quad \text{and} \quad g(z) = z.$$

Obviously, (14) follows (9), so x_s follows Definition 3.1.

By the splitting criteria (2), the optimal split of the stump can be found that

$$x_s^n = \operatorname{argmin}_{k \in \{1, \dots, C_x\}} \frac{1}{n} \left[\sum_{i=1}^{n_k} (y_{ki} - \bar{y}_k)^2 + \sum_{l \neq k} \left(\sum_{j=1}^{n_l} (y_{lj} - \bar{y}_{\bar{k}})^2 \right) \right],$$

where

$$\bar{y}_k = \frac{1}{n_k} \sum_{i=1}^{n_k} y_{ki} \quad \text{and} \quad \bar{y}_{\bar{k}} = \frac{1}{\sum_{l \neq k} n_l} \sum_{l \neq k} \sum_{j=1}^{n_l} y_{lj}.$$

Since we know that $n_k = \frac{1}{C_x}n$, $k = 1, \dots, C_x$. By the weak law of large numbers, we can prove that

$$\bar{y}_k \xrightarrow{p} \mu_k, \quad \bar{y}_{\bar{k}} \xrightarrow{p} \mu_{\bar{k}} \quad \text{as } n \rightarrow \infty.$$

So, with probability one,

$$\begin{aligned} \lim_{n \rightarrow \infty} x_s^n &= \operatorname{argmin}_{k \in \{1, \dots, C_x\}} \lim_{n \rightarrow \infty} \frac{1}{n} \left[\sum_{i=1}^{n_k} (y_{ki} - \bar{y}_k)^2 + \sum_{l \neq k} \left(\sum_{j=1}^{n_l} (y_{lj} - \bar{y}_{\bar{k}})^2 \right) \right] \\ &= \operatorname{argmin}_{k \in \{1, \dots, C_x\}} \lim_{n \rightarrow \infty} \frac{1}{n} \left[\sum_{i=1}^{n_k} (y_{ki} - \mu_k)^2 + \sum_{l \neq k} \left(\sum_{j=1}^{n_l} (y_{lj} - \mu_{\bar{k}})^2 \right) \right] = x_s. \end{aligned}$$

x_s^n converges to x_s in probability and the rate of convergence is $O(n^{-1})$. \square

Proof of Theorem 3.6. Let us construct that

$$p_{kj} = z^l(k), \quad \sum_{i \neq k} p_{ij} = z^r(k) \quad \text{and} \quad g(z(k)) = S_q(k).$$

Obviously, (15) follows (9), so x_s follows Definition 3.1.

By the splitting criteria (3), the optimal split of the stump can be found that

$$x_s^n = \operatorname{argmin}_{k \in \{1, \dots, C_x\}} [S_q^n(k) + S_q^n(\bar{k})],$$

where

$$\begin{aligned} S_q^n(k) &= \frac{1}{1-q} \left(\sum_{j=1}^{C_y} \left(\frac{1}{n_k} \sum_{l=1}^{n_k} I(y_l = j) \right)^q - 1 \right), \\ S_q^n(\bar{k}) &= \frac{1}{1-q} \left(\sum_{j=1}^{C_y} \left(\sum_{i \neq k} \left(\frac{1}{n_i} \sum_{m=1}^{n_i} I(y_m = j) \right) \right)^q - 1 \right), \quad i \in \{1, \dots, C_x\}, \quad q \in \mathbb{R}. \end{aligned}$$

Since we know that $n_k = \frac{1}{C_x}n$, $k = 1, \dots, C_x$. By Borel's law of large numbers, with probability one,

$$\lim_{n \rightarrow \infty} \frac{1}{n_k} \sum_{m=1}^{n_k} I(y_m = j) = p_{kj}, \quad k = 1, \dots, C_x, \quad j = 1, \dots, C_y.$$

So, with probability one,

$$\begin{aligned} \lim_{n \rightarrow \infty} x_s^n &= \operatorname{argmin}_{k \in \{1, \dots, C_x\}} \lim_{n \rightarrow \infty} [S_q^n(k) + S_q^n(\bar{k})] \\ &= \operatorname{argmin}_{k \in \{1, \dots, C_x\}} [S_q(k) + S_q(\bar{k})] = x_s. \end{aligned}$$

x_s^n converges to x_s in probability and the rate of convergence is $O(n^{-1})$. \square

B Supplementary materials

To empirically validate the theoretical results about the confidence interval (16), we conducted an experiment using a step function, denoted as $f(x)$, with a single optimal split at $x = 1$, as illustrated in panel (a) of Figure B.14. The experiment proceeded as follows:

- (1) At each sample size, we performed the following steps 1000 times:
 - Calculated the theoretical 95% confidence interval using (16).
 - Determined whether the true optimal split $x = 1$ falls within this interval.

We then calculated the coverage rate, which is the proportion of times the true optimal split was covered by the confidence interval.

- (2) We repeated step 1) a total of 100 times to obtain the empirical distribution of the coverage rate.

The results of this experiment are presented in panel (b) of Figure B.14. Notably, the empirical expectation of the coverage rate is approximately 95% when the sample size is 500 or larger. This empirical finding aligns well with the theoretical 95% confidence interval and supports the validity of confidence interval (16) and Lemma 3.2 in a practical context.

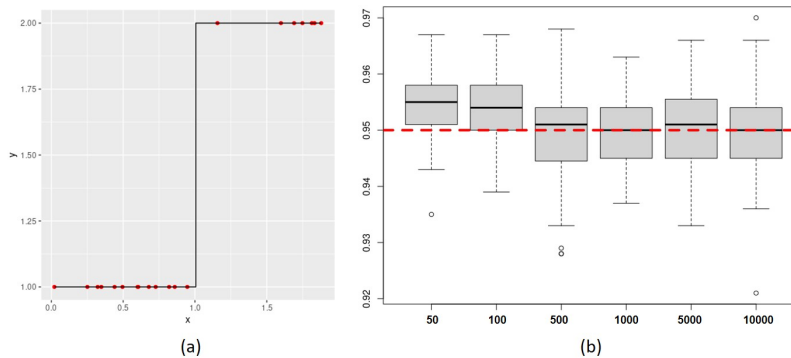


Figure B.14: (a) The true optimal split $x = 1$. (b) The coverage rate of 95% confidence intervals converges to the theoretical value (95%).

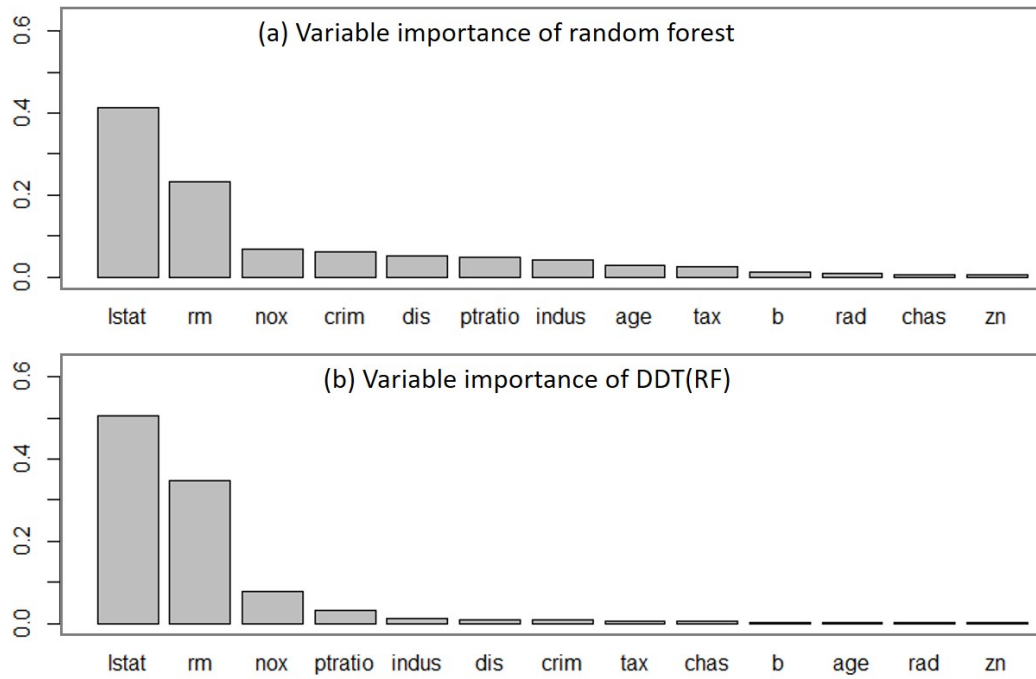


Figure B.15: Comparison of variable importance between the teacher Random Forest and the student DDT(RF).

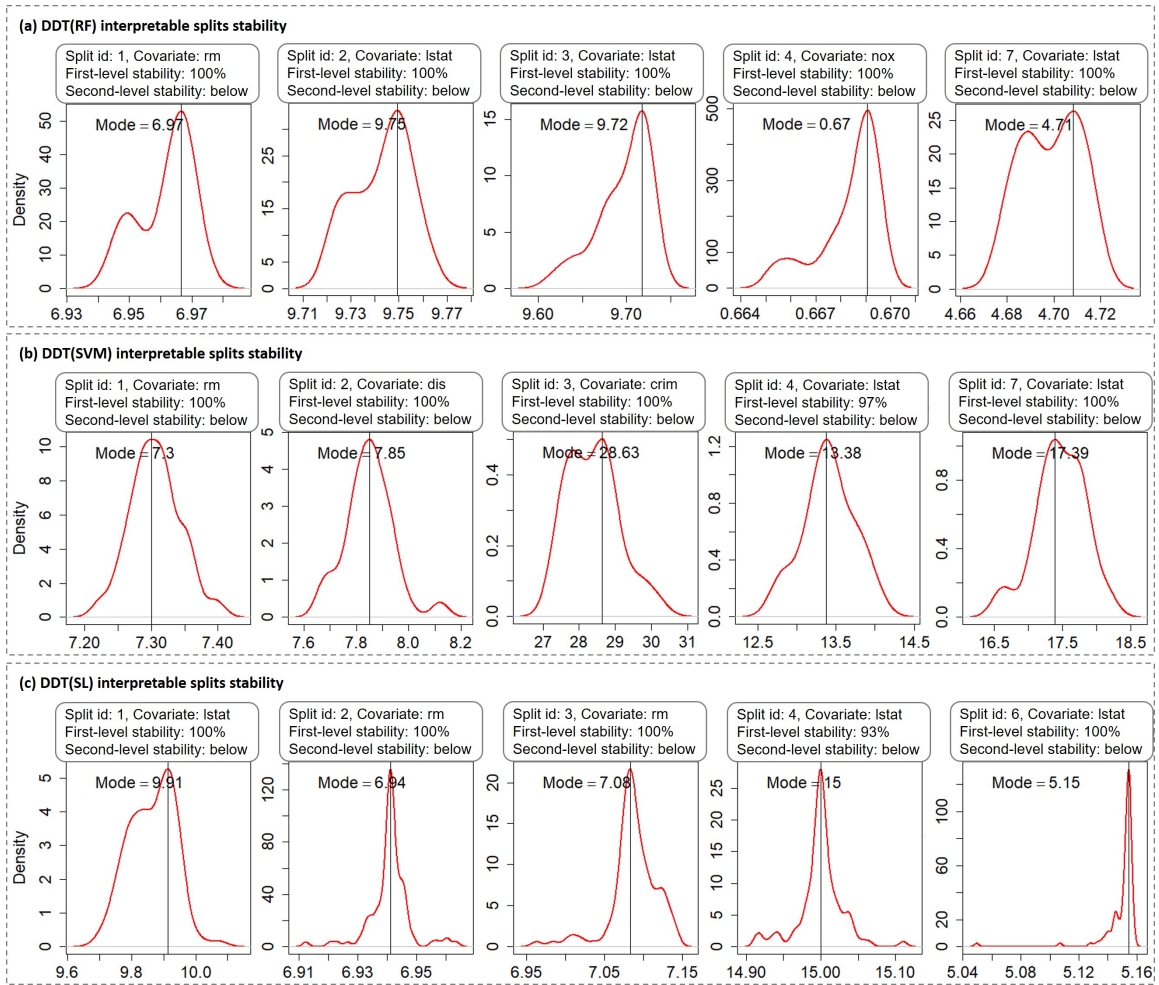


Figure B.16: Two-level stability of the interpretable splits in DDT(RF), DDT(SVM) and DDT(SL).

C Acknowledgments

The authors appreciate the helpful discussions with Dr. Wei-Ying Lou and the editorial assistance from Mrs. Jessica Swann.

D funding

J. Jack Lee's research was supported in part by the grants P30CA016672, P50CA221703, U24CA224285, and U24CA224020 from the National Cancer Institute, RP150519 and RP160668 from the Cancer Prevention and Research Institute of Texas, and The University of Texas MD Anderson Cancer Center Oropharynx Cancer Program generously supported by Mr. and Mrs. Charles W. Stiefel.

References

- Allen-Zhu, Z. and Y. Li (2021). Towards understanding ensemble, knowledge distillation and self-distillation in deep learning.
- Ba, J. and R. Caruana (2014). Do deep nets really need to be deep? In Z. Ghahramani, M. Welling, C. Cortes, N. Lawrence, and K. Q. Weinberger (Eds.), *Advances in Neural Information Processing Systems*, Volume 27. Curran Associates, Inc.
- Breiman, L. (2001). Statistical Modeling: The Two Cultures (with comments and a rejoinder by the author). *Statistical Science* 16(3), 199 – 231.
- Breiman, L., J. Friedman, C. J. Stone, and R. Olshen (1984). *Classification and Regression Trees*. Chapman and Hall/CRC.
- Bénard, C., G. Biau, S. da Veiga, and E. Scornet (2020). Interpretable random forests via rule extraction.
- Coppens, Y., K. Efthymiadis, T. Lenaerts, and A. Nowé (2019). Distilling deep reinforcement learning policies in soft decision trees. In *IJCAI 2019*.
- Cormen, T. H., C. E. Leiserson, R. L. Rivest, and C. Stein (2009). *Introduction to Algorithms, Third Edition* (3rd ed.). The MIT Press.
- Ding, Z., P. Hernandez-Leal, G. W. Ding, C. Li, and R. Huang (2021). Cdt: Cascading decision trees for explainable reinforcement learning.
- Frosst, N. and G. Hinton (2017). Distilling a neural network into a soft decision tree.
- Gou, J., B. Yu, S. J. Maybank, and D. Tao (2021, Mar). Knowledge distillation: A survey. *International Journal of Computer Vision* 129(6), 1789–1819.
- Hinton, G., O. Vinyals, and J. Dean (2015). Distilling the knowledge in a neural network. *arXiv preprint arXiv:1503.02531*.
- Hyafil, L. and R. L. Rivest (1976). Constructing optimal binary decision trees is np-complete. *Information Processing Letters* 5(1), 15–17.

- Johansson, U., C. Sönströd, and T. Löfström (2011). One tree to explain them all. In *2011 IEEE Congress of Evolutionary Computation (CEC)*, pp. 1444–1451.
- Laan, M. J. V. D., E. C. Polley, and A. E. Hubbard (2007). Super learner. *Statistical Applications in Genetics and Molecular Biology* 6(1), 25.
- Li, J., Y. Li, X. Xiang, S.-T. Xia, S. Dong, and Y. Cai (2020). Tnt: An interpretable tree-network-tree learning framework using knowledge distillation. *Entropy* 22(11).
- Lipkovich, I., A. Dmitrienko, and R. B. D’Agostino Sr. (2017). Tutorial in biostatistics: data-driven subgroup identification and analysis in clinical trials. *Statistics in Medicine* 36(1), 136–196.
- Quinlan, J. R. (1993). *C4.5: programs for machine learning*. San Francisco, CA, USA: Morgan Kaufmann Publishers Inc.
- Rokach, L. and O. Maimon (2014). *Data Mining With Decision Trees: Theory and Applications* (2nd ed.). USA: World Scientific Publishing Co., Inc.
- Shen, Y., X. Xu, and J. Cao (2020). Reconciling predictive and interpretable performance in repeat buyer prediction via model distillation and heterogeneous classifiers fusion. *Neural Comput. Appl.*
- Shi, Y., M.-Y. Hwang, X. Lei, and H. Sheng (2019). Knowledge distillation for recurrent neural network language modeling with trust regularization.
- Song, J., H. Zhang, X. Wang, M. Xue, Y. Chen, L. Sun, D. Tao, and M. Song (2021, June). Tree-like decision distillation. In *Proceedings of the IEEE/CVF Conference on Computer Vision and Pattern Recognition (CVPR)*, pp. 13488–13497.
- Stanton, S., P. Izmailov, P. Kirichenko, A. A. Alemi, and A. G. Wilson (2021). Does knowledge distillation really work?
- Urban, G., K. J. Geras, S. E. Kahou, O. Aslan, S. Wang, R. Caruana, A. Mohamed, M. Philipose, and M. Richardson (2017). Do deep convolutional nets really need to be deep and convolutional?

Wang, Y. and S.-T. Xia (2017). Unifying attribute splitting criteria of decision trees by tsallis entropy. In *2017 IEEE International Conference on Acoustics, Speech and Signal Processing (ICASSP)*, pp. 2507–2511.

Zhou, Y., Z. Zhou, and G. Hooker (2018). Approximation trees: Statistical stability in model distillation.